

GL-TR-89-0346

2

REMOTE SOUNDING OF ATMOSPHERIC TEMPERATURE
PROFILES USING THE OPTICAL MEASURE METHOD

S. C. Ou
K. N. Liou

AD-A244 828



Center for Atmospheric and Remote Sounding Studies (CARSS)
Department of Meteorology
University of Utah
Salt Lake City, Utah 84112

31 December 1989

Final Report
12 September 1988 - 31 December 1989

DTIC
ELECTE
JAN 15 1992
S B D

Approved for public release; distribution unlimited


GEOPHYSICS LABORATORY
AIR FORCE SYSTEMS COMMAND
UNITED STATES AIR FORCE
HANSCOM AFB, MASSACHUSETTS 01731-5000

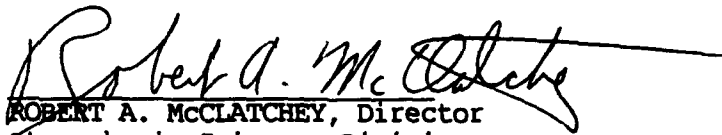
92 1 14 008

92-01226



This technical report has been reviewed and is approved for publication.


JEAN I.F. KING
Contract Manager
Atmospheric Sciences Division


ROBERT A. McCLATCHEY, Director
Atmospheric Sciences Division

This report has been reviewed by the ESD Public Affairs Office (PA) and is releasable to the National Technical Information Service (NTIS).

Qualified requestors may obtain additional copies from the Defense Technical Information Center. All others should apply to the National Technical Information Service.

If your address has changed, or if you wish to be removed from the mailing list, or if the addressee is no longer employed by your organization, please notify PL/TSI, Hanscom AFB, MA 01731-5000. This will assist us in maintaining a current mailing list.

Do not return copies of this report unless contractual obligations or notices on a specific document requires that it be returned.

UNCLASSIFIED

SECURITY CLASSIFICATION OF THIS PAGE

REPORT DOCUMENTATION PAGE

1a REPORT SECURITY CLASSIFICATION Unclassified			1b RESTRICTIVE MARKINGS		
2a SECURITY CLASSIFICATION AUTHORITY			3 DISTRIBUTION AVAILABILITY OF REPORT		
2b DECLASSIFICATION DOWNGRADING SCHEDULE			Approved for public release; distribution unlimited.		
4 PERFORMING ORGANIZATION REPORT NUMBER(S)			5 MONITORING ORGANIZATION REPORT NUMBER(S)		
			GL-TR-89-0346		
6a NAME OF PERFORMING ORGANIZATION Center for Atmospheric and Remote Sounding Studies		6b OFFICE SYMBOL (If applicable) CARSS		7a NAME OF MONITORING ORGANIZATION Geophysics Laboratory	
6c ADDRESS (City, State and ZIP Code) Department of Meteorology/CARSS University of Utah Salt Lake City, Utah 84112		7b ADDRESS (City, State and ZIP Code) Hanscom Air Force Base Bedford, Massachusetts 01731-5000			
8a NAME OF FUNDING SPONSORING ORGANIZATION		8b OFFICE SYMBOL (If applicable)		9 PROCUREMENT INSTRUMENT IDENTIFICATION NUMBER F19628-88-K-0049	
8c ADDRESS (City, State and ZIP Code)		10 SOURCE OF FUNDING NOS			
		PROGRAM ELEMENT NO		PROJECT NO.	TASK NO.
		61102F		2310	G8
11 TITLE (Include Security Classification) Remote Sounding of Atmospheric Temperature Profiles Using the...		WORK UNIT NO. AF			
12 PERSONAL AUTHOR(S) S. C. Ou, K. N. Liou					
13a TYPE OF REPORT Final		13b TIME COVERED FROM 9/12/88 TO 12/31/89		14 DATE OF REPORT (Yr, Mo, Day) 31 December 1989	
15 PAGE COUNT 68					
16 SUPPLEMENTARY NOTATION					
17 COSATI CODES			18 SUBJECT TERMS (Continue on reverse if necessary and identify by block number)		
FIELD	GROUP	SUB GR	Remote Sensing, Inversion Theory, Optical Measure Method, Differential Inversion Method, HIRS, Temperature Retrieval		
19 ABSTRACT (Continue on reverse if necessary and identify by block number)					
<p>This report describes an exploratory investigation on the applicability of the Optical Measure Method (OMM) to the retrieval of atmospheric temperature profiles using both the simulated and HIRS-2 radiances. We first present the basic theory of the OMM. Then we describe the synthetic retrieval of temperature profiles using HIRS-2 channels. Without performing an adjustment to the radiances, temperature profiles derived from both polynomial and polynomial-hyperbolic functional fitting of radiances are poor. We identify two major sources of errors through a forward analysis. One is the variation in the sharpness index of the weighting function with sounding channels, while the other is the surface contribution to radiances. For these reasons, an adjustment scheme has been developed using the concept of "scaling factors", which encompasses the effects of variation in the sharpness index, surface discontinuity, channel properties, and functional forms. Retrieved temperature profiles derived from</p>					
20 DISTRIBUTION AVAILABILITY OF ABSTRACT UNCLASSIFIED UNLIMITED <input checked="" type="checkbox"/> SAME AS RPT <input type="checkbox"/> DTIC USERS <input type="checkbox"/>			21 ABSTRACT SECURITY CLASSIFICATION Unclassified		
22a NAME OF RESPONSIBLE INDIVIDUAL Jean I. F. King			22b TELEPHONE NUMBER (617) 377-2977		22c OFFICE SYMBOL LY

UNCLASSIFIED

UNCLASSIFIED

SECURITY CLASSIFICATION OF THIS PAGE

polynomial-hyperbolic functional fitting of adjusted radiances are much improved. We show that the Differential Inversion Method (DIM) for temperature retrieval and OMM are mathematically equivalent. In practice, the DIM works better because of the fitting of radiances in the logarithmic pressure scale, which accounts for some of the surface contribution. Application of the DIM to an archive of 3473 collocated temperature profiles and radiance data sets shows that the accuracy of the retrieved temperatures is within about 3 K below 250 mb. In order to obtain a better accuracy, modifications and refinements are required for the DIM.

Continuation of block 11: Optical Measure Method.



Accession For	
NTIS GRA&I	<input checked="checked" type="checkbox"/>
DTIC TAB	<input type="checkbox"/>
Unannounced	<input type="checkbox"/>
Justification	
By	
Distribution/	
Availability Codes	
Dist	Avail and/or Special

TABLE OF CONTENTS

	<u>Page</u>
Section 1	
INTRODUCTION	1
Section 2	
OPTICAL-MEASURE THEORY	3
2.1 Polynomial Method	3
2.2 Optical Number System	5
2.3 Nonlinear Hyperbolic Method	7
Section 3	
APPLICATIONS OF THE OMM TO TEMPERATURE RETRIEVALS USING THE HIRS CHANNELS	9
3.1 Determining of Weighting Functions and Radiances	9
3.2 Fitting of Radiance	11
3.2.1 Formulation of the PH Function	19
3.2.2 Prescription of m_1 and m_2	22
3.2.3 A Least-Square Algorithm	22
3.3 Direct Application of the OMM Without Adjustments	25
3.4 A Forward Analysis on the OMM	26
3.5 Application of the OMM with Adjustments	34
3.6 Optimum Functional Form for the Planck Intensity Profile	38
Section 4	
COMPARISONS BETWEEN THE DIM AND THE OMM	44
4.1 The Equivalence Between the DIM and the OMM	44
4.2 Preliminary Applications of the DIM and HIRS Data	47
Section 5	
CONCLUSIONS	52
REFERENCES	55
APPENDIX	56

Section 1

INTRODUCTION

There are numerous schemes that are available for the retrieval of temperature profiles. In most inversion approaches, certain *a priori* assumptions on the temperature profile or constraints on its variation are required. The root mean square (rms) errors of the retrieved temperature profile from the traditional methods vary between 1 and 5 K (Phillips et al. 1988). The external restrictions generally take the form of an initial trial profile and the departure allowed from the initial guess is restricted. The methods with *a priori* constraints may work well in an average sense but large errors may result in extreme cases.

The inference of atmospheric temperature profile should be based on the solution of the radiative transfer equation. The formal solution of the radiative transfer equation is represented by the Fredholm integral equation of the first kind. There are problems involving the instability of the solution and the ill-conditioned property of the equation itself, since in practice the data available for the performance of inversion are finite. Because the number of unknowns are more than the number of equations, the solutions are not unique.

King (1985) proposed a differential inversion method (DIM), in which the Planck intensity at pressure levels corresponding to the peaks of weighting functions can be directly expressed in terms of the sum of the derivatives of upwelling radiances in the logarithmic pressure coordinate. This inversion technique that does not involve *a priori* assumptions was developed based on the Laplace transform of the integral equation. In the follow-up effort, King (1987)

developed a similar retrieval algorithm referred to as the optical measure method (OMM). The fundamental principle of both the DIM and OMM is that no initial guess of the temperature profile or a prescription of specific constraints is needed. The two methods represent pioneering efforts to break away from conventional techniques. In the OMM, a certain functional form is needed to represent the Planck intensity profile.

In our previous report, we have explored the generalization and applicability of the DIM by way of a synthetic study (Liou, et al. 1989). We showed that the retrieved temperatures at the lower four peak pressure levels of HIRS channels 4-7 are accurate to within 2 K. In this report, we present a similar investigation on the OMM. In Section 2, the theoretical foundations for the OMM are presented. Applications of the OMM to synthetic radiances of the HIRS 15 μm CO₂ channels for temperature retrievals are described in Section 3. Subsequently, the advantages and shortcomings the DIM and OMM are discussed in Section 4. Finally, conclusions are given in Section 5.

Section 2

OPTICAL MEASURE METHOD

2.1 Polynomial Method

It is assumed that the radiance and Planck profiles are continuous and differentiable over the optical pressure (\bar{p}) and atmospheric pressure (p) spaces, respectively, where \bar{p} is the pressure corresponding to the peak of the weighting function. It is associated with the absorption properties of spectral bands. We may express the radiance over a certain spectral band with the mean wavenumber $\bar{\nu}$ in terms of a polynomial function of \bar{p} as follows:

$$R[\bar{p}(\bar{\nu})] = r_0 + r_1\bar{p} + r_2\bar{p}^2 + \dots = \sum_{\ell=0}^{\infty} r_{\ell} \bar{p}^{\ell} \quad (2.1)$$

The corresponding Planck function may also be expressed in terms of a polynomial of p in the form

$$B_{\bar{\nu}}(p) = b_0 + b_1p + b_2p^2 + \dots = \sum_{\ell=0}^{\infty} b_{\ell} p^{\ell} \quad (2.2)$$

Based on the formal solution of the radiative transfer equation that is applied to a plane-parallel atmosphere (Chandrasekhar, 1950), the radiance is related to the Planck function in the form

$$R[\bar{p}(\bar{\nu})] = \int_0^{\infty} B_{\bar{\nu}}(p) W_{\bar{\nu}}(p/\bar{p}) dp/p \quad (2.3)$$

where $W_{\bar{\nu}}(p/\bar{p})$ is the weighting function for a certain spectral band, which is defined as

$$W_{\nu}(p/\bar{p}) = \frac{dT_{\nu}(p/\bar{p})}{d(\ln p)} \quad , \quad (2.4)$$

and $T_{\nu}(p/\bar{p})$ is the transmittance from the level p to the top of atmosphere. We substitute Eqs. (2.1) and (2.2) into Eq. (2.3) to obtain

$$\sum_{\ell=0}^{\infty} r_{\ell} \bar{p}^{\ell} = \sum_{\ell=0}^{\infty} b_{\ell} \bar{p}^{\ell} \int_0^{\infty} \bar{p}'^{\ell-1} W_{\nu}(\bar{p}) d\bar{p} \quad , \quad (2.5)$$

where $\bar{p} = p/\bar{p}$. The coefficients for the Planck function can now be determined by matching the terms of equal power in \bar{p} . Thus,

$$b_{\ell} = r_{\ell} \left[\int_0^{\infty} \bar{p}'^{\ell-1} W_{\nu}(\bar{p}) d\bar{p} \right]^{-1} \quad (2.6)$$

and the Planck function can be written as

$$B_{\nu}(p) = \sum_{\ell=0}^{\infty} r_{\ell} \left[\int_0^{\infty} \bar{p}'^{\ell-1} W_{\nu}(\bar{p}) d\bar{p} \right]^{-1} \bar{p}^{\ell} \quad . \quad (2.7)$$

Equation (2.7) implies that the Planck function can be inferred through a polynomial expression of p if the coefficients r_{ℓ} are determinable. At present, the number of sensing channels on board satellites are limited. For example, the HIRS-2 radiometer has only seven channels in the $15 \mu\text{m}$ CO_2 band for temperature retrievals. If we use the data from these channels, the degree of polynomial expansions cannot exceed six because the coefficients of higher-degree polynomials are not unique.

Even with all the values of r_{ℓ} known, another obstacle inherent in the method is the determination of the integral in Eq. (2.6). Although the integration from $p = 0$ to $p = \infty$ could be carried out numerically, its accuracy would be highly questionable. King (1987) proposed a new "optical number system" to resolve the problem of integration analytically.

2.2 Optical Number System

According to King (1985), the weighting function can be expressed in a generalized form:

$$W(\tilde{p}) = \frac{\kappa^{(\kappa-1)/\kappa}}{\Gamma(1/\kappa)} \tilde{p} \exp(-\tilde{p}^\kappa/\kappa) \quad , \quad (2.8)$$

where κ is the "sharpness index", and Γ the Gamma function. Two special cases can be derived from this generalized weighting function. For $\kappa = 1$,

$$W(\tilde{p}) = \tilde{p} \exp(-\tilde{p}) \quad . \quad (2.9)$$

This expression corresponds to the weighting function derived from the Goody-Mayer random model. On the other hand, for $\kappa = 2$, we have

$$W(\tilde{p}) = \sqrt{2/\pi} \tilde{p} \exp(-\tilde{p}^2/2) \quad , \quad (2.10)$$

This corresponds to the weighting function derived from the Elsasser band model.

Using the generalized weighting function, integration in Eq. (2.5) may be done analytically. Using properties of the Gamma function, we obtain

$$\begin{aligned} \int_0^\infty \tilde{p}^{\ell-1} W_{\tilde{p}}(\tilde{p}) d\tilde{p} &= \frac{\kappa^{(\kappa-1)/\kappa}}{\Gamma(1/\kappa)} \int_0^\infty \tilde{p}^\ell \exp(-\tilde{p}^\kappa/\kappa) d\tilde{p} \\ &= \frac{\kappa^{\ell/\kappa} \Gamma[(\ell+1)/\kappa]}{\Gamma(1/\kappa)} \end{aligned} \quad (2.11)$$

A generalized Gamma function may be defined in the form

$$\Gamma_\kappa(\ell+1) = \frac{\kappa^{\ell/\kappa} \Gamma[(\ell+1)/\kappa]}{\Gamma(1/\kappa)} \quad . \quad (2.12)$$

In this manner, Eq. (2.7) may be expressed by

$$B_{\tilde{p}}(p) = \sum_{\ell=0}^{\infty} r_\ell [\Gamma_\kappa(\ell+1)]^{-1} p^\ell \quad . \quad (2.13)$$

When $\kappa \rightarrow 1$, the generalized Gamma function is reduced to the form of Gamma function in terms of natural number system. Since the Gamma function has the following property:

$$\Gamma(l+1) = l \Gamma(l) \quad , \quad \text{for} \quad l = 1, 2, 3, \dots \quad (2.14)$$

we can also construct an optical number system n_κ , such that

$$\Gamma_\kappa(l+1) = l_\kappa \Gamma_\kappa(l) \quad , \quad \text{for} \quad l = 1, 2, 3, \dots \quad (2.15)$$

This optical number system reflects the ratio of successive moment integrals of the weighting function, i.e.

$$l_\kappa = \frac{\int_0^\infty \bar{p}^l \exp(-\bar{p}^\kappa/\kappa) d\bar{p}}{\int_0^\infty \bar{p}^{l-1} \exp(-\bar{p}^\kappa/\kappa) d\bar{p}} \quad (2.16)$$

For $\kappa > 1$, which corresponds to a sharper weighting function with larger $W_{\nu, \max}$ and steeper slope on either side of the peak, $l < l_\kappa$. For $\kappa < 1$, $l_\kappa > l$. The parameter l_κ may be referred to as the sub-natural and super-natural number systems for $l_\kappa < l$ and $l_\kappa > l$, respectively. For retrieval purposes, the sub-natural number system is desired, because sharper weighting functions would give more accurate retrieval results (Liou and Ou, 1989).

In practice, there is a weighting function profile for each sounding channel. A distinctive value of κ can be assigned to each channel by fitting the generalized form to the weighting function. Thus, if we evaluate $B_{\nu}^-(p)$ according to Eq. (2.7), we will obtain several values of $B_{\nu}^-(p)$ that correspond to different κ . A conversion of $B_{\nu}^-(p)$ to temperature may not lead to a uniform κ value at the same pressure level. To determine a mean temperature profile, a weighting method is usually used (Smith, 1970).

2.3 Nonlinear Hyperbolic Method

The key to the success of the OMM lies in the adequate fitting of a finite number of radiance measurements by a smooth function of a combination of smooth functions. Higher-degree polynomials may fit every radiance data point well, but they may also carry spurious oscillations between data points. This will lead to unrealistic solutions of the Planck function. Thus, we are forced to seek the fitting of radiances that will not produce unnecessary wiggles between data points, but at the same time the fitted curve will match each data point with reasonable accuracy.

One possible candidate for the radiance fitting is the nonlinear hyperbolic function. According to Chandrasekhar (1950), the upwelling intensity from a plane-parallel atmosphere can be expressed as a sum of hyperbolic functions. Thus, $R[\bar{p}(\bar{\nu})]$ may be expressed in the form

$$R[\bar{p}(\bar{\nu})] = \sum_{j=0}^{\infty} \frac{\tilde{r}_j}{1+m_j\bar{p}} \quad (2.17)$$

Actually, Eq. (2.17) is equivalent to a combination of geometrical series:

$$\sum_{j=0}^{\infty} \frac{\tilde{r}_j}{1+m_j\bar{p}} = \sum_{j=0}^{\infty} \tilde{r}_j [1 - m_j\bar{p} + (m_j\bar{p})^2 - \dots] \quad (2.18)$$

Comparing Eq. (2.18) with Eq. (2.1), we note that

$$r_l = \sum_{j=0}^{\infty} \tilde{r}_j (-m_j)^l \quad (2.19)$$

and the coefficients of the Planck function are given by

$$b_l = \frac{r_l}{l_{\kappa}!} = \sum_{j=0}^{\infty} \frac{\tilde{r}_j (-m_j)^l}{l_{\kappa}!} \quad (2.20)$$

Substituting Eq. (2.20) into Eq. (2.2) yields

$$B_{\nu}(p) = \sum_{j=0}^{\infty} \sum_{\ell=0}^{\infty} \frac{\tilde{r}_j (-m_j)^{\ell}}{\ell_{\kappa}!} p^{\ell} \quad (2.21)$$

By exchanging the order of summation in Eq. (2.21), we find

$$B_{\nu}(p) = \sum_{j=0}^{\infty} \tilde{r}_j \sum_{\ell=0}^{\infty} \frac{(-m_j)^{\ell}}{\ell_{\kappa}!} p^{\ell} = \sum_{j=0}^{\infty} \tilde{r}_j e^{-m_j p} \quad (2.22)$$

for $\kappa = 1$. The Planck function is now given by a linear combination of exponential functions with different arguments. We may define an optical exponential function such that

$$\exp_{\kappa}(x) = \sum_{\ell=0}^{\infty} x^{\ell} / \ell_{\kappa}! \quad (2.23)$$

It follows that Eq. (2.21) may be generalized in the form

$$B_{\nu}(p) = \sum_{j=0}^{\infty} \tilde{r}_j \exp_{\kappa}(-m_j p) \quad (2.24)$$

Using the combination of hyperbolic expressions for radiances, we obtain a series expansion of B_{ν} in terms of the optical exponential function. Evaluation of the optical exponential function must be done through Eq. (2.23). For $\kappa = 1$, this equation reduces to the exponential function.

Section 3

APPLICATIONS OF THE OMM TO TEMPERATURE RETRIEVALS

USING THE HIRS CHANNELS

In this section, we shall present the results of applying the OMM to temperature retrievals by performing synthetic analyses using the properties of HIRS channels in the 15 μm CO_2 band.

3.1 Determination of Weighting Functions and Radiances

There are seven channels in the HIRS 15 μm CO_2 band with central wavenumbers at 668, 679, 690, 702, 716, 732, and 748 cm^{-1} . The smaller wavenumber corresponds to broader weighting functions with maxima located at higher altitudes. The last two channels are also affected by the absorption/emission due to water vapor. Details of the channel characteristics are listed in Table 1.

Table 1. HIRS Channel Characteristics

Channel	ν (cm^{-1})	ν_1	ν_2	$\Delta\nu$	Principal Absorbers	Level of W_{max}
1	668	666	670	4	CO_2	30
2	679	674	684	10	CO_2	60
3	690	685	697	12	CO_2	100
4	702	696	712	16	CO_2	250
5	716	708	724	16	CO_2	500
6	732	724	740	16	$\text{CO}_2/\text{H}_2\text{O}$	750
7	748	740	756	16	$\text{CO}_2/\text{H}_2\text{O}$	900

We used the CO₂ absorption coefficients computed by Chou and Kouvaris (1986) based on line-by-line data compiled by Rothman et al. (1983) to compute transmittances and weighting functions, using the k-correlated method. This method transforms the spectral integral over the wavenumber space into an integral over the domain of the accumulated frequency distribution of the absorption coefficient. Furthermore, to account for the inhomogeneous atmosphere, we assume that the variation in the absorption coefficient depends only on pressure and temperature so that the frequency distributions of the absorption coefficient can be correlated through pressure and temperature. In practice, we use the cumulated frequency distribution (g) look-up table to determine the relationship between the absorption coefficient at an arbitrary level and that at the reference level. The reference absorption coefficient is determined from each g value. The spectral transmittance is obtained by numerical integration over the g space (Liou and Ou, 1988).

A numerical method was developed to fit the HIRS weighting functions to the generalized form denoted in Eq. (2.8) to obtain the sharpness index, κ , associated with each channel. It is similar to the least-square method. However, the quantity that is to be minimized is the weighted square sum of errors. More weight is placed on the error near the peak of the weighting function, because a significant portion of the upwelling radiance comes from emission near the peak level. The resulting nonlinear algebraic equation is solved by Newton's iteration method. The sharpness index of the fitted weighting functions for Channels 1-7 are 0.49, 1.56, 1.50, 2.19, 2.34, 4.34, and 3.16 respectively. Except channel 1, the κ values associated with all other channels are larger than 1. The κ value deviates from 1 and 2, implying that neither the Goody random band model nor the Elsasser regular band model can properly simulate

the total transmittance in the 15 μm CO_2 band. The errors for the fitted weighting functions are within ± 0.02 . Since the fitting method places more weight on minimizing errors near the peaks than in the wings, the percentage errors near the peaks ($< 2\%$) is much smaller than those in the wing regions. Figures 1(a)-(g) show the weighting functions computed from the k-correlated method and the fitted generalized weighting functions. The fitting for Channel 1 is not as satisfactory as those for other channels, due to the secondary peak above 10 mb. The figures also show that the weighting function of Channel 1 is much broader than other channels. Channels 6 and 7 are the sharpest channels with peaks close to the surface. The fitted weighting functions for these two channels are slightly broader than those computed from the k-correlated method. The present results were obtained by the systematic optimization method, and therefore can be applied to any weighting function.

The channel radiance values were then obtained from synthetic computations. We used the US Standard Atmospheric Temperature Profile and evaluate the radiances according to Eq. (2.3). The generalized weighting functions were used. Table 2 lists the computed upwelling radiances for the first seven HIRS channels. We notice that these radiances increase from the band center (Channels 2 and 3) to the band wing (Channels 6 and 7).

3.2 Fitting of Radiance

The seven upwelling radiances were fitted to either a 5th-degree polynomial function or a combined polynomial-hyperbolic (PH) function. In the case of the 5th-degree polynomial fitting, we used the subroutine DRCURV in the International Mathematical and Statistical Library (IMSL). The resulting curve is shown in Fig. 2 as the solid line. There are two reasons for choosing the 5th-degree polynomial. For a lower-degree polynomial, the fitting will not be exact. On the

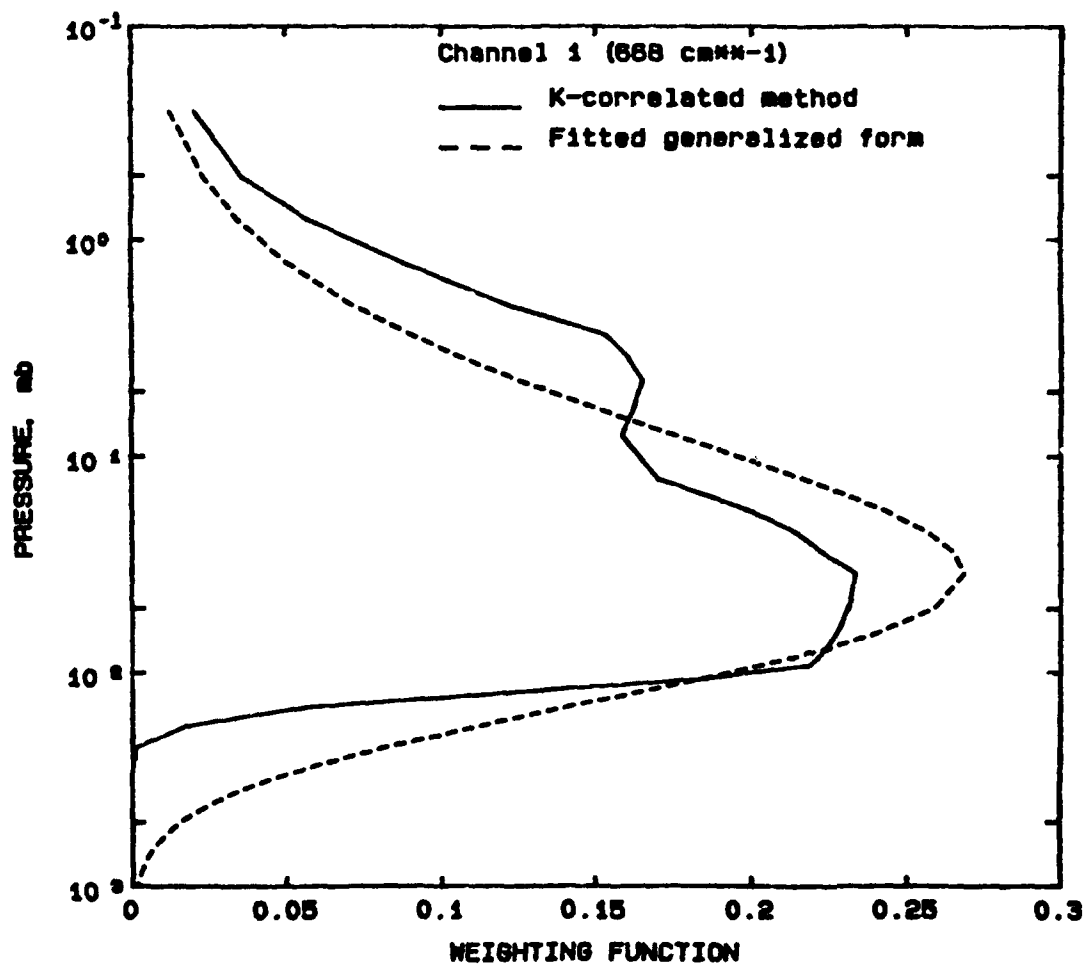


Fig. 1(a). The weighting function of HIRS-2 Channel 1. The solid and dashed lines represent results computed from the correlated k-distribution method and the generalized weighting function, respectively.

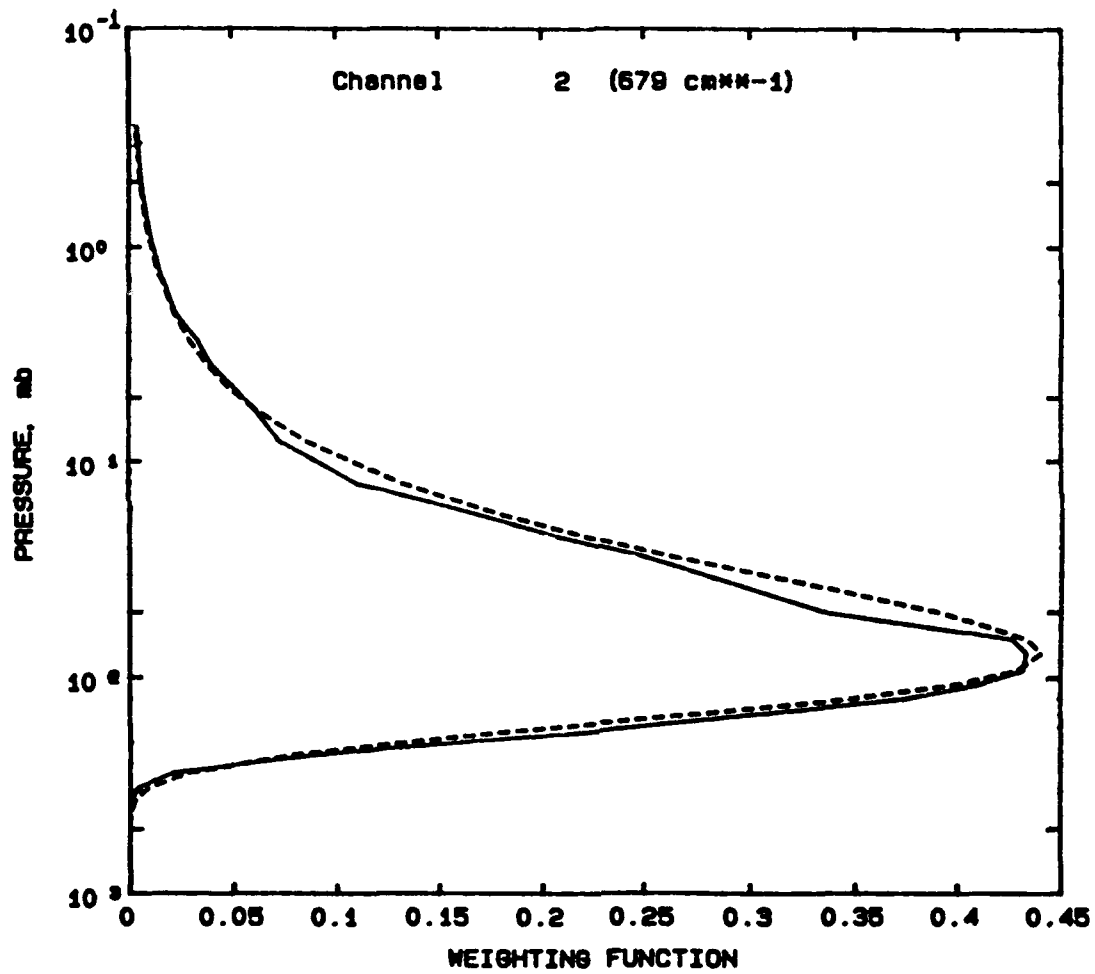


Fig. 1(b). Same as Fig. 1(a), except for HIRS-2 Channel 2.

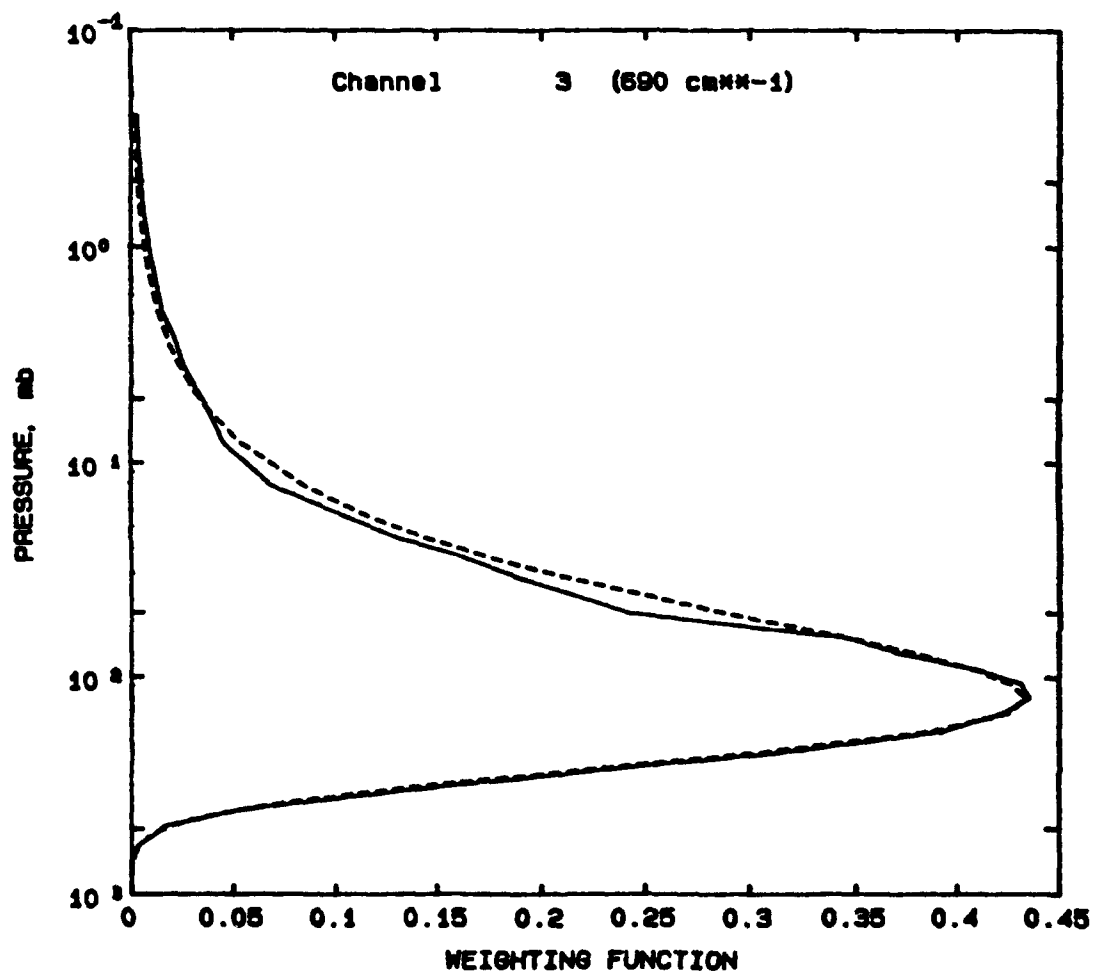


Fig. 1(c). Same as Fig. 1(a), except for HIRS-2 Channel 3.

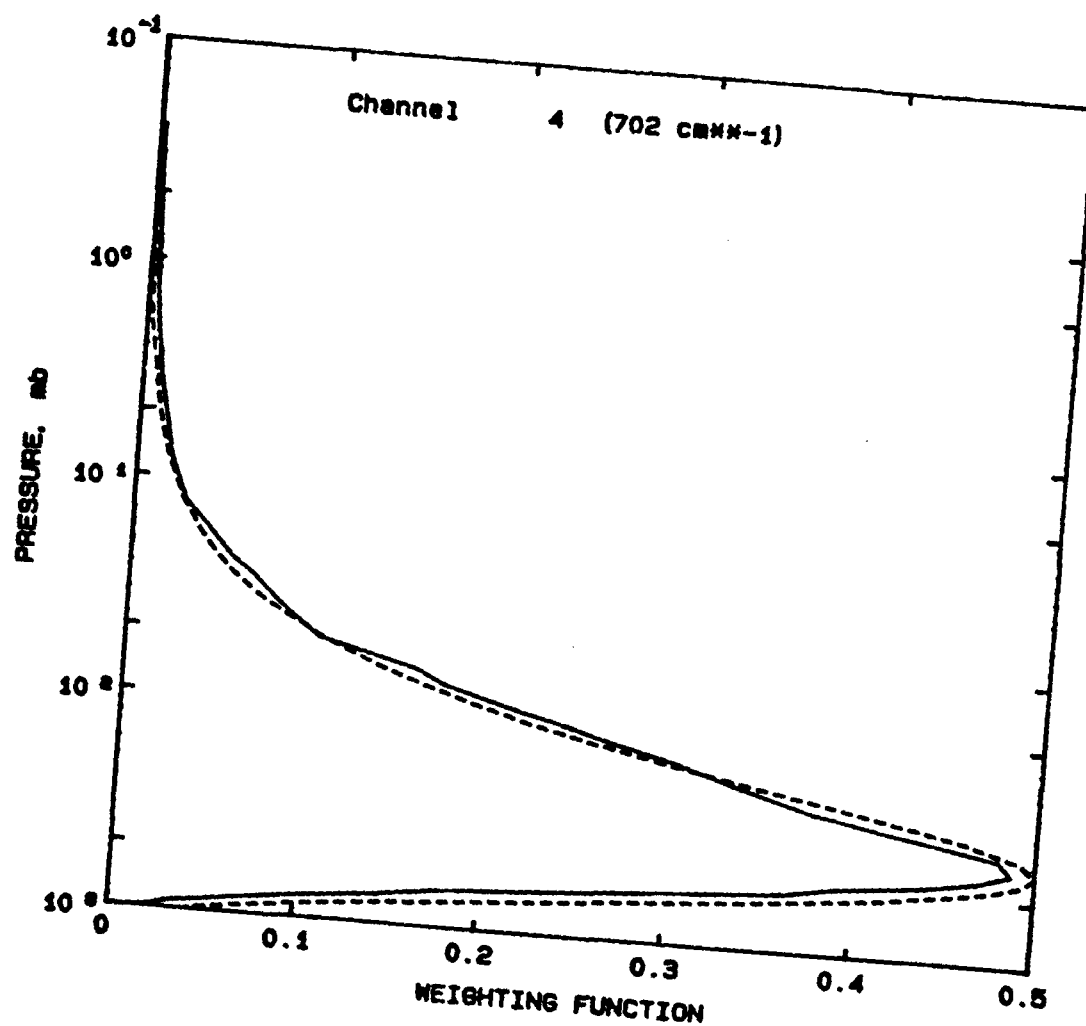


Fig. 1(d). Same as Fig. 1(a), except for HIRS-2 Channel 4.

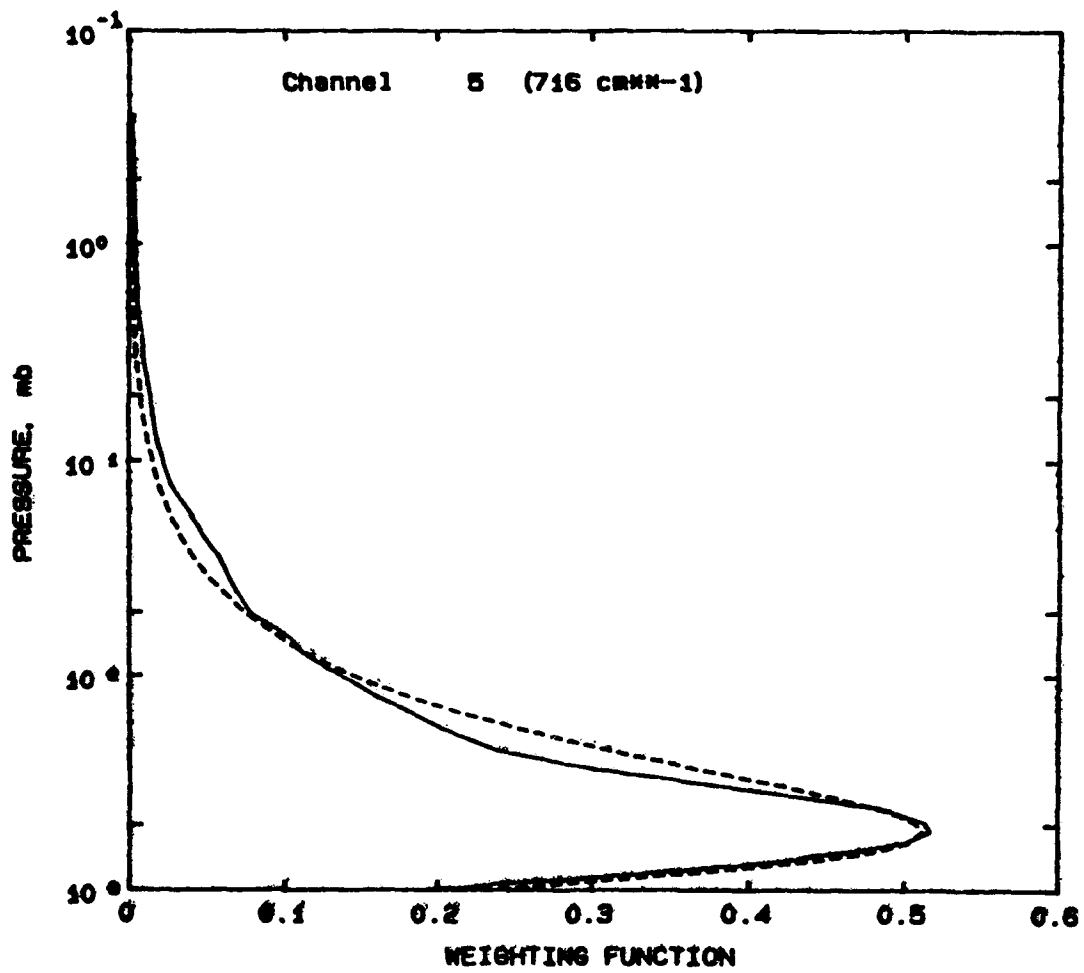


Fig. 1(e). Same as Fig. 1(a), except for HIRS-2 Channel 5.

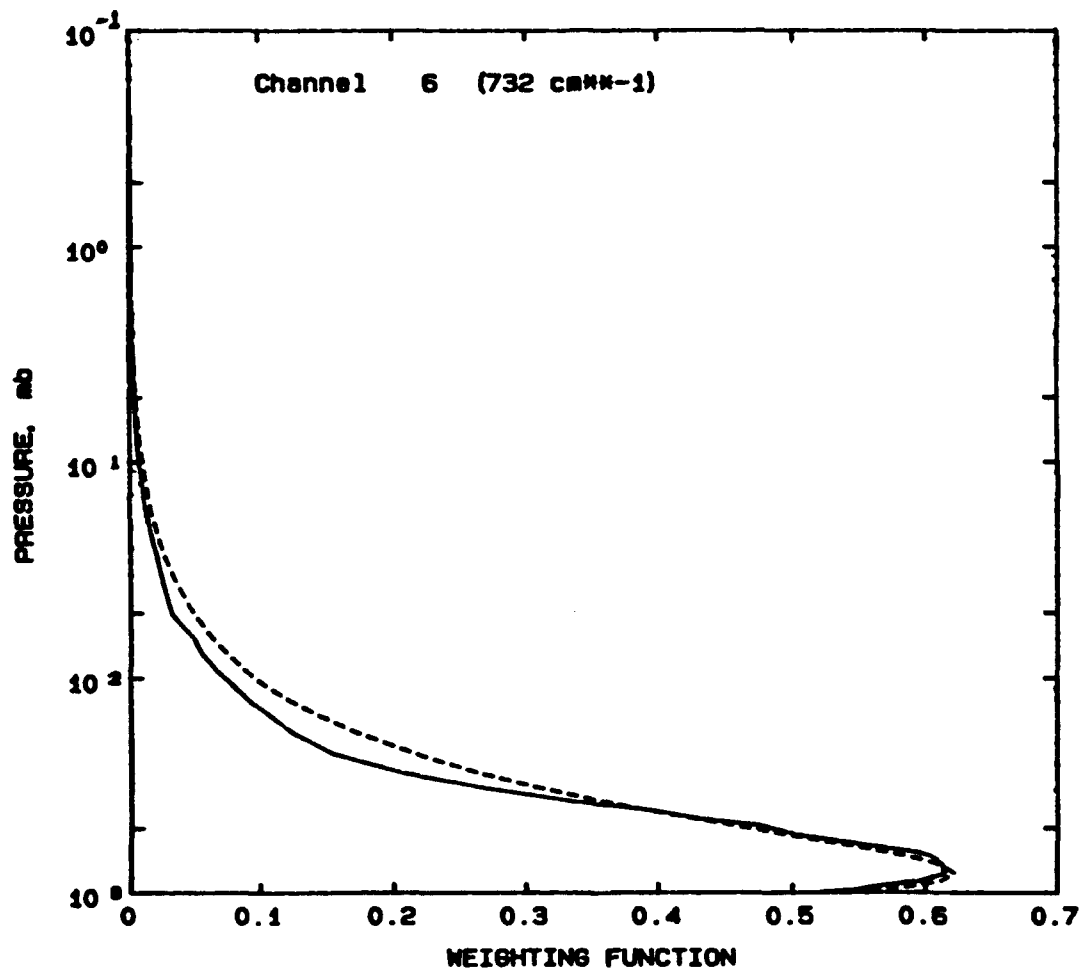


Fig. 1(f). Same as Fig. 1(a), except for HIRS-2 Channel 6.

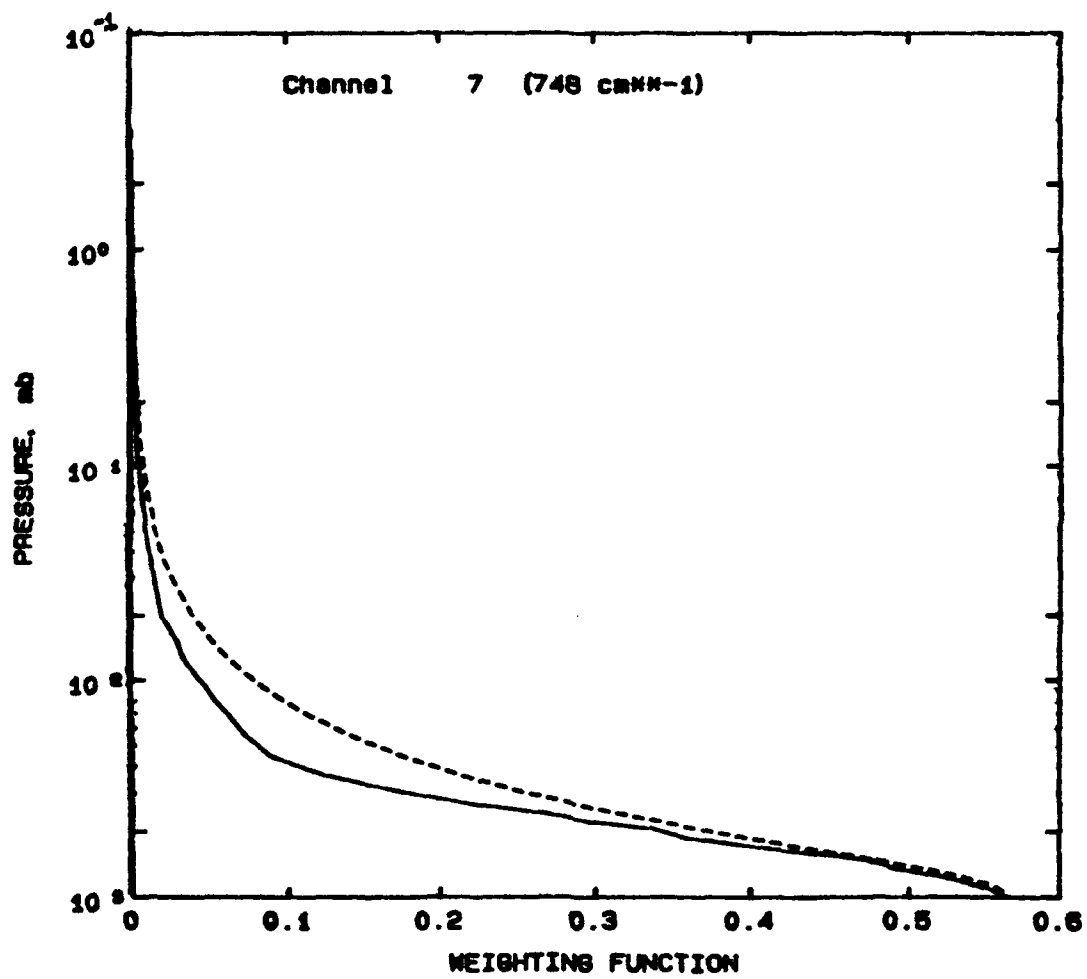


Fig. 1(g). Same as Fig. 1(a), except for HIRS-2 Channel 7.

Table 2. Radiance values for HIRS channels.

Channel	Radiance (erg/cm ² -cm ⁻¹ -sec-sr)
1	53.5
2	46.0
3	44.4
4	54.9
5	60.1
6	70.6
7	78.2

other hand, for a higher-degree polynomial, there will be unrealistic oscillations between data points. Figure 2 shows that the fitted curve has a local minimum between $\bar{p} = 100$ and 200 mb. The curve fits almost exactly to all the radiances except those of Channels 2 and 3. In addition, there are slight but noticeable oscillations between Channels 4 and 7.

In the case of fitting the radiances to the PH function, we have developed an algorithm based on the principle of the least-square method. This is described in the following subsections.

3.2.1 Formulation of the PH Function

The combined PH function can be written as follows:

$$\bar{R}[\bar{p}(\bar{\nu})] = \sum_{\ell=1}^{N_1} r_{\ell} \bar{p}^{\ell-1} + \sum_{\ell=1}^{N_2} \frac{L_{\ell}}{1+m_{\ell}\bar{p}}, \quad (2.1)$$

which is a combination of Eq. (2.1) and (2.17). The selection of such a form was based on reasons related to the distribution of radiances. Since the peak of the Channel 1 weighting function is well within the stratosphere, in which the temperature is generally near isothermal or increases with altitude, the measured

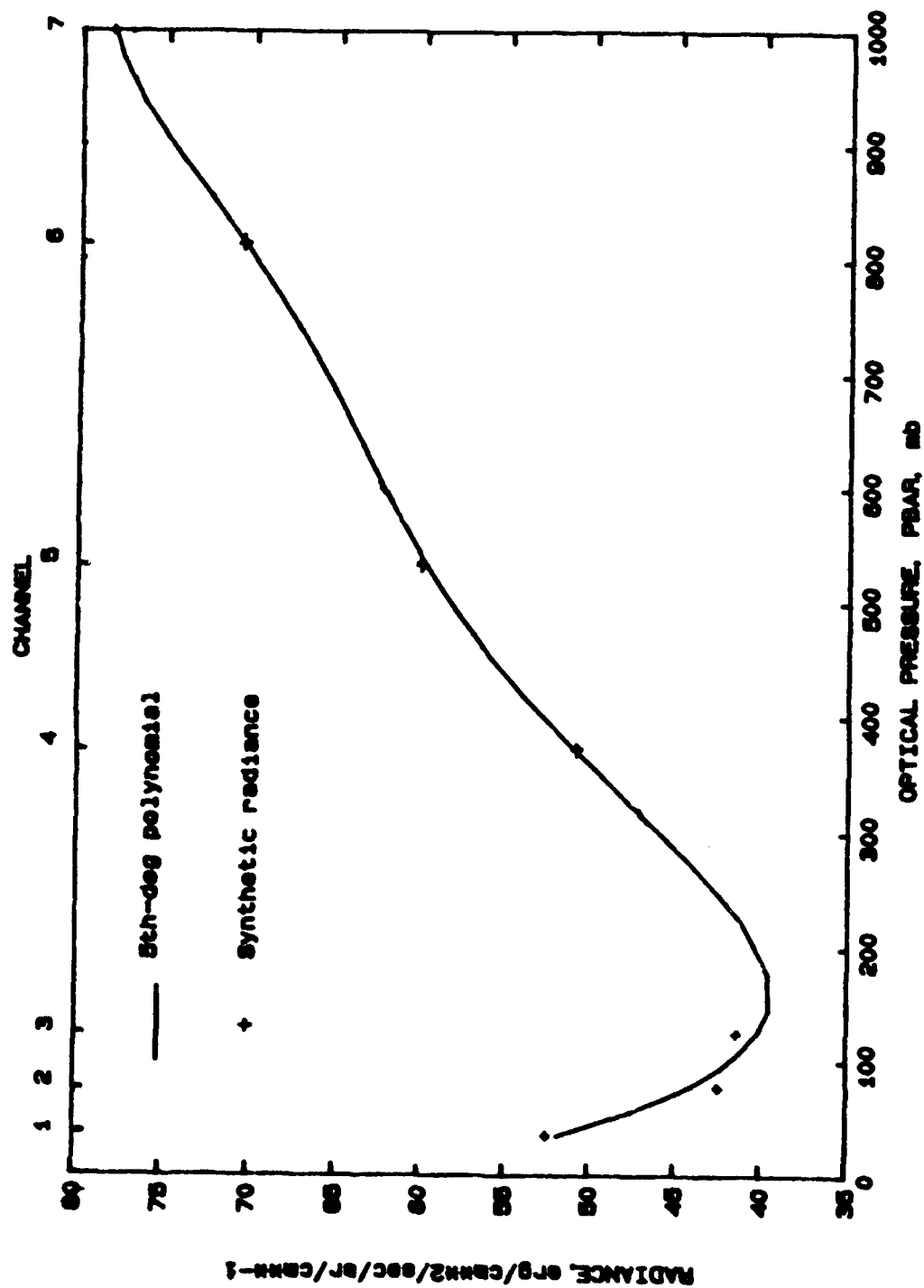


Fig. 2. The fitting of a 5th-order polynomial (solid line) and a polynomial-hyperbolic function (dashed line) to the synthetic radiances for the seven HIRS-2 channels. The US Standard Atmosphere Temperature profile was used in synthetic computations.

Channel 1 radiance is usually higher than Channel 2 radiance. The radiances increase from Channel 3 to Channel 7 as the peaks of the weighting function gradually lower toward surface. The corresponding temperature at the peak increases. Usually, radiances measured by Channel 2 or Channel 3 are the smallest. This implies that the fitted curve must be able to generate such local minima. Thus, a second- or higher-degree polynomial is required. However, as the degree of the fitted polynomial increases, so does the amplitude of fluctuation between data point, which may cause serious instability on the solution. An alternative is to fit the radiances to a series of non-linear hyperbolic functions denoted in Eq. (2.17). However, our preliminary studies show that the resultant fittings based on the least-square principle are far from satisfactory. One serious defect is that it cannot reproduce the local minimum of Channel 2 radiances, because the functional form $1/(1 + x)$ is monotonous on either side of $x = -1$.

Finally, we find that the combined PH function can simulate the local minimum, and at the same time it meets the smoothness requirement. Since the number of data points in the present case is seven, the fitting should have no more than seven undetermined coefficients. If the number of unknown coefficients exceeds seven, the fitting is not unique unless additional constraints are imposed. Thus, for best fitting, we can have only three combinations: (1) $N_1 = 1$, $N_2 = 3$ (7 unknowns), (2) $N_1 = N_2 = 2$ (6 unknowns), and (3) $N_1 = 3$, $N_2 = 2$ (7 unknowns). As stated above, case (1) is the sum of pure hyperbolic functions, which cannot reproduce the local minimum. At present, we have selected case (2) as a preliminary test of the functional form since the coefficients in this case can be easily determined.

3.2.2 Prescription of m_1 and m_2

From Eq. (3.1), let $N_1 = N_2 = 2$. We have

$$\bar{R}[\bar{p}(\bar{\nu})] = r_1 + r_2 \bar{p} + \frac{L_1}{1 + m_1 \bar{p}} + \frac{L_2}{1 + m_2 \bar{p}} , \quad (3.2)$$

where r_1 , r_2 , L_1 , L_2 , m_1 , and m_2 are coefficients to be determined.

Equation (3.2) is a non-linear function, if m_1 and m_2 are considered to be unknown coefficients. However, if we prescribe m_1 and m_2 , then it becomes a linear combination of three functional forms with one constant. The remaining coefficients can be found from a least-square method. In general, m_1 and m_2 can be real numbers from $-\infty$ to $+\infty$. Fortunately, by carefully reviewing the derivation of the retrieval formula, we find that in order for the method to be mathematically consistent, m_1 and m_2 must be within a certain range. We notice that the equality,

$$\frac{1}{1+x} = 1 - x + x^2 - x^3 \dots = \sum_{l=0}^{\infty} (-x)^l , \quad (3.3)$$

is valid only when $|x| < 1$. Applying this restriction to Eq. (2.18), we conclude that $|m_1 \bar{p}|$ and $|m_2 \bar{p}|$ must be less than 1, or $|m_1|$ and $|m_2|$ must be less than $1/\bar{p}$. Otherwise, Eqs. (2.18) and (2.24) will not be valid. Since \bar{p} ranges between 0 and 1000 mb, $|m_1|$ and $|m_2|$ have to be less than 10^{-3} . This small range allows us to pre-select a few values of m_1 and m_2 within this range to compute the best-fit coefficients in Eq. (3.2) and the corresponding rms error.

3.2.3 A Least-Square Algorithm

Based on Eq. (3.2), the square sum of the difference between the fitted and the actual values of $R[\bar{p}(\bar{\nu})]$ may be expressed by

$$E = \sum_{j=1}^7 (r_1 + r_2 \bar{p}_j + \frac{L_1}{1 + m_1 \bar{p}_j} + \frac{L_2}{1 + m_2 \bar{p}_j} - R_j)^2 \quad (3.4)$$

To minimize E, we set the partial differentials with respect to the coefficients to zero, vis.,

$$\frac{\partial E}{\partial r_1} = \frac{\partial E}{\partial r_2} = \frac{\partial E}{\partial L_1} = \frac{\partial E}{\partial L_2} = 0 \quad (3.5)$$

This minimization process leads to a system of four linear equations, which can be expressed in the following matrix form:

$$\begin{bmatrix} 7 & \bar{P} & \bar{X}_1 & \bar{X}_2 \\ \bar{P} & \bar{P}^2 & \bar{X}_1 \bar{P} & \bar{X}_2 \bar{P} \\ \bar{X}_1 & \bar{X}_1 \bar{P} & \bar{X}_1^2 & \bar{X}_1 \bar{X}_2 \\ \bar{X}_2 & \bar{X}_2 \bar{P} & \bar{X}_1 \bar{X}_2 & \bar{X}_2^2 \end{bmatrix} \begin{bmatrix} r_1 \\ r_2 \\ L_1 \\ L_2 \end{bmatrix} = \begin{bmatrix} \bar{R} \\ \bar{R} \bar{P} \\ \bar{R} \bar{X}_1 \\ \bar{R} \bar{X}_2 \end{bmatrix} \quad (3.6)$$

where

$$\bar{X}_1 = \sum_{j=1}^7 1/(1 + m_1 \bar{p}_j) \quad , \quad i = 1, 2 \quad ,$$

$$\bar{X}_1^2 = \sum_{j=1}^7 1/(1 + m_1 \bar{p}_j)^2 \quad , \quad i = 1, 2 \quad ,$$

$$\bar{X}_1 \bar{X}_2 = \sum_{j=1}^7 1/[(1 + m_1 \bar{p}_j) (1 + m_2 \bar{p}_j)] \quad ,$$

$$\bar{P} = \sum_{j=1}^7 \bar{p}_j \quad ,$$

$$\bar{P}^2 = \sum_{j=1}^7 \bar{p}_j^2 \quad ,$$

$$\overline{X_i P} = \sum_{j=1}^7 \bar{p}_j / (1 + m_i \bar{p}_j), \quad i = 1, 2, \quad ,$$

$$\bar{R} = \sum_{j=1}^7 R_j \quad ,$$

$$\overline{R P} = \sum_{j=1}^7 R_j \bar{p}_j \quad ,$$

$$\overline{R X_i} = \sum_{j=1}^7 R_j / (1 + m_i \bar{p}_j) \quad , \quad i = 1, 2 \quad .$$

Solution of r_1 , r_2 , L_1 , and L_2 depends on the prescribed value of m_1 and m_2 . The rms error is defined by

$$e = \sqrt{E/7} \quad . \quad (3.7)$$

Since the values of m_1 and m_2 should be between -10^{-3} and 10^{-3} , we select six representative values: $\pm 3.5 \times 10^{-4}$, $\pm 6.5 \times 10^{-4}$, and $\pm 9.5 \times 10^{-4}$. For each pair of m_1 and m_2 , we may solve the linear system of Eq. (3.6) and compute the rms error from Eq. (3.7). The idea is to determine which pair of (m_1, m_2) produce minimum rms error. Table 3 lists the rms error for all pairs of (m_1, m_2) using the synthetic radiances listed in Table 2. Clearly, Table 3 shows that the rms error is generally smaller for $m_1 m_2 < 0$ (one negative) than for $m_1 m_2 > 0$ (both positive or negative). Furthermore, for the case $m_1 m_2 < 0$, the rms error for the pair of (m_1, m_2) is the same as for the pair of (m_2, m_1) . The minimum rms error is 2.8 for $m_1 = 9.5 \times 10^{-4}$ and $m_2 = -3.5 \times 10^{-4}$, and the coefficients in this case are $r_1 = 79.6$, $r_2 = 0.498$, $L_1 = 445$ and $L_2 = -473$. The fitted PH function is also shown in Fig. 2 as the dashed line. Although the general fitting of the PH

Table 3. The root-mean-square error of radiances for selected pairs of (m_1, m_2)

$m_2 \times 10^4$	$m_1 \times 10^4$					
	-9.5	-6.5	-3.5	3.5	6.5	9.5
-9.5	4.2	3.8	3.7	3.5	3.4	3.4
-6.5	3.8	4.1	3.5	3.3	3.2	3.1
-3.5	3.7	3.6	3.9	3.2	2.9	2.8
3.5	3.5	3.3	3.2	3.7	23.4	13.9
6.5	3.4	3.2	2.9	8.5	3.7	4.6
9.5	3.4	3.1	2.8	5.1	3.2	3.6

function is less satisfactory than the polynomial function, particularly near the local minimum, the PH function is smoother than the polynomial function. Better fittings can be obtained with $|m_i| > 1$ (Leon and King, 1989). However, as noted above, the series will not converge and the OMM is not mathematically valid in this case.

3.3 Direct Application of OMM Without Adjustments

Retrieval exercises were carried out based on the two functional forms for radiances. Planck functions derived from the polynomial form can be written as

$$B(\bar{\nu}_i, p) = \sum_{\ell=1}^6 \frac{r_{\ell} p^{\ell-1}}{(\ell-1)_{\kappa}!}, \quad (3.8)$$

where κ is associated with the i th channel. Planck functions based on the PH form can be written as a combination of polynomial and optical-exponential

functions as follows:

$$B(\bar{\nu}_1, p) = r_1 + r_2 p / 1_{\kappa}! + L_1 \exp_{\kappa}(-m_1 p) + L_2 \exp_{\kappa}(-m_2 p) \quad (3.9)$$

In this way, since there are seven channels, each with a different value for κ , we may obtain seven profiles for $B(\bar{\nu}_1, p)$. Each Planck profile can be converted to a temperature profile $T(\bar{\nu}_1, p)$. We used the method of weighted average (Smith, 1970) to obtain the final temperature profile as follows:

$$\bar{T}(p) = \frac{\sum_{i=1}^7 [W(\bar{\nu}_i, p) T(\bar{\nu}_i, p)]}{\sum_{i=1}^7 W(\bar{\nu}_i, p)} \quad (3.10)$$

Figure 3 shows the retrieved temperature profiles based on Eqs. (3.8) and (3.9), along with the reference standard temperature profile. Both retrieved profiles deviate significantly from the standard temperature profile. The profile derived from the PH function is better than that from the polynomial. A further examination of the figure reveals that the profile from the PH function is colder by 5-12 K below 250 mb but warmer by 0-5 K above this pressure level.

In an attempt to investigate the reason for discrepancies, we found two problems that need to be resolved in order for the OMM to be practical for temperature retrievals. The first problem is related to the variation in κ , while the second is associated with the discontinuity of the temperature profile. These problems were identified through a forward-analysis procedure which will be described in the following subsection.

3.4 A Forward Analysis on the OMM

In this section, a forward analysis will be performed to illustrate the reasons for the deviation of the retrieved temperature profile from the standard temperature profile.

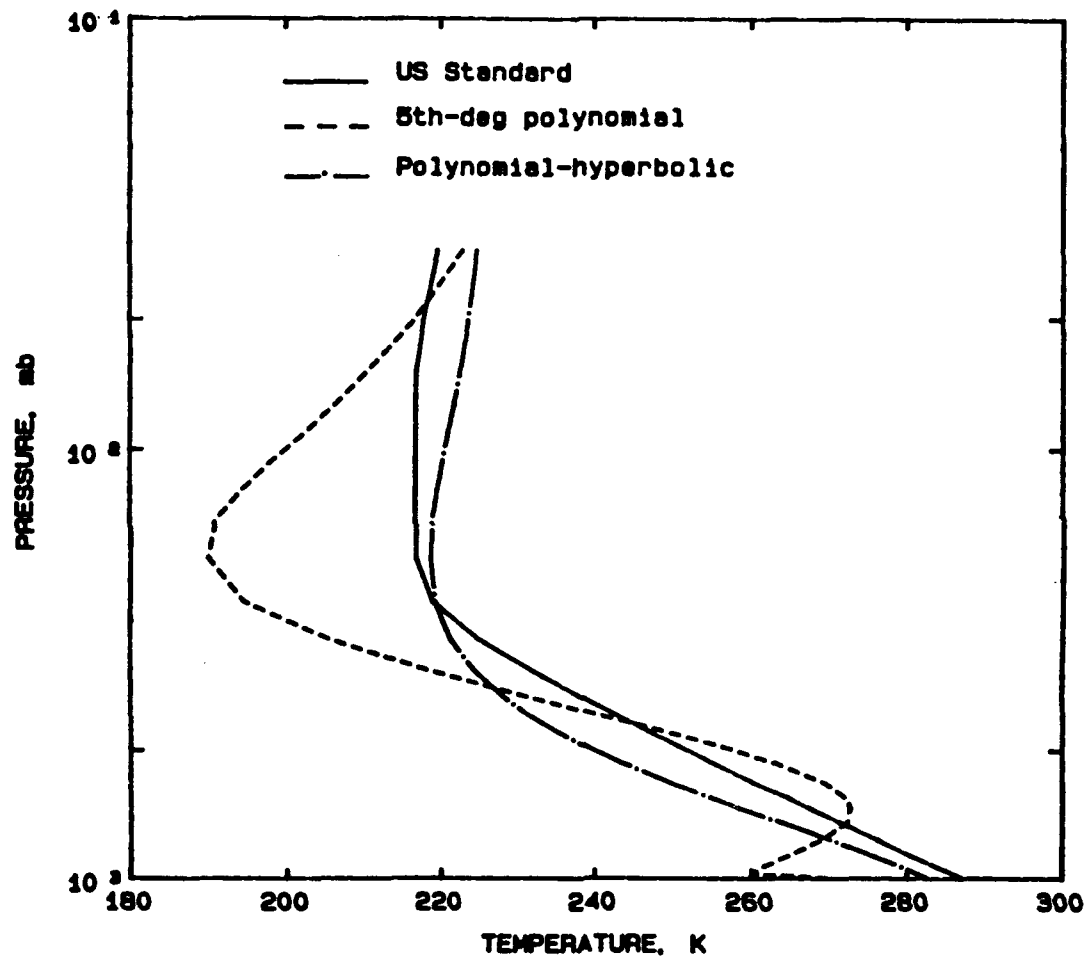


Fig. 3. Retrieved temperature profiles based on the fitting of synthetic radiances shown in Fig. 2.

According to the description in Section 2, the Planck profile can be represented by either polynomial functions or optical exponential functions or a combination of the two as shown by Eq. (3.9). It is not known how well such functional forms can match the Planck profiles. In the previous subsection, we demonstrated that the PH function yields better retrieval results than the polynomial function. For this reason the PE function defined by Eq. (3.9) is chosen to fit the standard Plank profile.

Given that m_1 and m_2 are prescribed, we use the least-square method similar to the one described in Sec. 3.2.3 to perform numerical fittings. We first define a square sum of errors as

$$E = \sum_j^N [r_1 + r_2 p_j / 1_{\kappa}! + L_1 \exp_{\kappa}(-m_1 p_j) + L_2 \exp_{\kappa}(-m_2 p_j) - B_j]^2 \quad (3.11)$$

Performing the minimization procedure, we obtain the following linear system:

$$\begin{bmatrix} N & \bar{\Pi} & \bar{\chi}_1 & \bar{\chi}_2 \\ \bar{\Pi} & \bar{\Pi}^2 & \bar{\chi}_1 \bar{\Pi} & \bar{\chi}_2 \bar{\Pi} \\ \bar{\chi}_1 & \bar{\chi}_1 \bar{\Pi} & \bar{\chi}_1^2 & \bar{\chi}_1 \bar{\chi}_2 \\ \bar{\chi}_2 & \bar{\chi}_2 \bar{\Pi} & \bar{\chi}_1 \bar{\chi}_2 & \bar{\chi}_2^2 \end{bmatrix} \begin{bmatrix} r_1 \\ r_2 \\ L_1 \\ L_2 \end{bmatrix} = \begin{bmatrix} \bar{B} \\ \bar{B} \bar{\Pi} \\ \bar{B} \bar{\chi}_1 \\ \bar{B} \bar{\chi}_2 \end{bmatrix} \quad (3.12)$$

where

$$\bar{\chi}_i = \sum_{j=1}^N \exp_{\kappa}(-m_i p_j) \quad , \quad i = 1, 2 \quad ,$$

$$\bar{\chi}_i^2 = \sum_{j=1}^N \exp_{\kappa}(-m_i p_j)^2 \quad , \quad i = 1, 2 \quad ,$$

$$\bar{\chi}_1 \bar{\chi}_2 = \sum_{j=1}^N \exp_{\kappa}(-m_1 p_j) \exp_{\kappa}(-m_2 p_j) \quad ,$$

$$\bar{\Pi} = \sum_{j=1}^N p_j / l_{\kappa}! ,$$

$$\overline{\Pi^2} = \sum_{j=1}^N (p_j / l_{\kappa}!)^2 ,$$

$$\overline{\chi_i \Pi} = \sum_{j=1}^N p_j \exp_{\kappa}(-m_i p_j) , \quad i = 1, 2 ,$$

$$\bar{B} = \sum_{j=1}^N B_j ,$$

$$\overline{B \Pi} = \sum_{j=1}^N B_j \bar{p}_j / l_{\kappa}! ,$$

$$\overline{B \chi_i} = \sum_{j=1}^N B_j \exp_{\kappa}(-m_i p_j) , \quad i = 1, 2 ,$$

In computing the preceding matrix elements, the evaluation of the optical exponential function was done by the series summation method according to Eq. (2.23). We found that about 15 terms are sufficient for the series to converge to a constant number. Since each channel has a different Planck intensity profile, and since the optical exponential function varies with the sharpness index κ , the coefficients r_1 , r_2 , L_1 , and L_2 depend on both the spectral band of each channel for κ . For the seven HIRS channels, there are 49 sets of coefficients. These coefficients are listed in Table 4. It is evident that for the same κ , the coefficients vary slightly with channels. However, for the same channel, the coefficients depend strongly on κ . Also, these sets of values are different from the values in Section 3.2.3. The first problem can now be stated

Table 4. Coefficients of the fitted polynomial-hyperbolic functional form for the seven HIRS channels in terms of different sharpness indices, κ

Channel		κ						
		0.49	1.56	1.50	2.19	2.34	4.34	3.16
1	r_1	0.315E+04	0.131E+04	0.186E+04	0.632E+03	0.575E+03	0.187E+03	0.336E+03
	r_2	0.250E+01	0.146E+01	0.195E+01	0.933E+00	0.894E+00	0.537E+00	0.690E+00
	L_1	0.989E+03	0.818E+03	0.107E+04	0.598E+03	0.585E+03	0.413E+03	0.493E+03
	L_2	-0.409E+04	-0.208E+04	-0.288E+04	-0.118E+04	-0.112E+04	-0.554E+03	-0.783E+03
2	r_1	0.306E+04	0.130E+04	0.184E+04	0.626E+03	0.560E+03	0.183E+03	0.331E+03
	r_2	0.236E+01	0.145E+01	0.154E+01	0.928E+00	0.890E+00	0.534E+00	0.886E+00
	L_1	0.911E+03	0.816E+03	0.107E+04	0.598E+03	0.583E+03	0.411E+03	0.491E+03
	L_2	-0.393E+04	-0.207E+04	-0.286E+04	-0.118E+04	-0.111E+04	-0.548E+03	-0.778E+03
3	r_1	0.302E+04	0.128E+04	0.182E+04	0.617E+03	0.560E+03	0.179E+03	0.325E+03
	r_2	0.236E+01	0.144E+01	0.193E+01	0.923E+00	0.883E+00	0.531E+00	0.681E+00
	L_1	0.950E+03	0.813E+03	0.106E+04	0.593E+03	0.580E+03	0.410E+03	0.489E+03
	L_2	-0.409E+04	-0.205E+04	-0.285E+04	-0.117E+04	-0.110E+04	-0.545E+03	-0.770E+03
4	r_1	0.287E+04	0.127E+04	0.181E+04	0.606E+03	0.549E+03	0.173E+03	0.319E+03
	r_2	0.240E+01	0.143E+01	0.191E+01	0.913E+00	0.874E+00	0.526E+00	0.676E+00
	L_1	0.973E+03	0.808E+03	0.105E+04	0.588E+03	0.576E+03	0.407E+03	0.486E+03
	L_2	-0.405E+04	-0.203E+04	-0.281E+04	-0.115E+04	-0.108E+04	-0.539E+03	-0.762E+03
5	r_1	0.287E+04	0.125E+04	0.178E+04	0.596E+03	0.540E+03	0.168E+03	0.312E+03
	r_2	0.218E+01	0.141E+01	0.189E+01	0.904E+00	0.866E+00	0.521E+00	0.669E+00
	L_1	0.957E+03	0.799E+03	0.105E+04	0.584E+03	0.572E+03	0.404E+03	0.482E+03
	L_2	-0.368E+04	-0.201E+04	-0.279E+04	-0.114E+04	-0.107E+04	-0.532E+03	-0.753E+03
6	r_1	0.287E+04	0.122E+04	0.175E+04	0.581E+03	0.528E+03	0.162E+03	0.302E+03
	r_2	0.227E+01	0.139E+01	0.186E+01	0.891E+00	0.854E+00	0.513E+00	0.658E+00
	L_1	0.970E+03	0.790E+03	0.103E+04	0.577E+03	0.566E+03	0.399E+03	0.477E+03
	L_2	-0.362E+04	-0.197E+04	-0.274E+04	-0.112E+04	-0.105E+04	-0.522E+03	-0.740E+03
7	r_1	0.271E+04	0.120E+04	0.171E+04	0.568E+03	0.514E+03	0.155E+03	0.293E+03
	r_2	0.223E+01	0.138E+01	0.184E+01	0.879E+00	0.841E+00	0.506E+00	0.650E+00
	L_1	0.984E+03	0.784E+03	0.102E+04	0.571E+03	0.558E+03	0.395E+03	0.471E+03
	L_2	-0.363E+04	-0.195E+04	-0.270E+04	-0.110E+04	-0.103E+04	-0.512E+03	-0.727E+03

as follows: "Due to the variation in the sharpness index with the channel, it appears not practical to use only one set of coefficients to represent all the measured radiances."

Since each radiance value corresponds to a different κ , using a single set of coefficients to represent all the radiances as has been shown in Subsection 3.2.3 would produce large temperature errors. In the retrieval exercise described in Subsection 3.3, none of the retrieved temperature profiles is close to the standard profile.

To show how well the PH function defined by Eq. (3.11) fits the input Planck intensity profile, the rms errors for the Planck function and temperature are presented in Table 5. Also in this table are temperature rms errors. For $\kappa < 1$, the fitting is poor because the matrix approaches singular. On the other hand, for $\kappa > 2$, the temperature rms errors are on the order of 1.2 - 2.0 K. This indicates that the PE function is potentially useful to produce real atmospheric Planck profiles.

Next, we examine the errors in the radiances generated by the fitted Planck profile. We compute three sets of "radiances". The first is based on the input Planck profile with a contribution from the surface separate from the integral as follows:

$$R_1(\bar{p}_1) = B_{\nu}(p_s) T_{\nu}(p/\bar{p}_1) + \int_0^{p_s} B_{\nu}(p) W_{\nu}(\kappa_1, p/\bar{p}_1) dp/p \quad (3.13)$$

Note that Eq. (3.13) is equivalent to Eq. (2.3), if the temperature for $p > p_s$ is assumed to be isothermal. The second set of radiances was obtained from the following equation:

$$R_1(\bar{p}_1) = B_{\nu}(p_s) T_{\nu}(p/\bar{p}_1) + \int_0^{p_s} B_{\nu}(p) W_{\nu}(\kappa_1, p/\bar{p}_1) dp/p \quad (3.14)$$

Table 5. The rms error for the fitting of Planck profiles of the first seven HIRS channels in terms of different sharpness indices, κ

Channel	κ						
	0.49	1.56	1.50	2.19	2.34	4.34	3.16
1 $\overline{\Delta B}$	19.1	1.9	4.1	1.5	1.5	1.5	1.5
$\overline{\Delta T}$	14.6	1.7	3.5	1.4	1.3	1.3	1.3
2 $\overline{\Delta B}$	9.5	1.7	2.1	2.1	1.5	1.5	1.5
$\overline{\Delta T}$	7.4	1.5	1.7	2.0	1.4	1.3	1.3
3 $\overline{\Delta B}$	**	2.7	6.2	1.4	1.6	1.4	1.5
$\overline{\Delta T}$	**	2.4	5.6	1.3	1.5	1.3	1.3
4 $\overline{\Delta B}$	**	1.7	2.9	1.5	1.6	1.4	1.4
$\overline{\Delta T}$	**	1.7	2.4	1.4	1.5	1.3	1.3
5 $\overline{\Delta B}$	**	1.5	1.7	1.4	1.4	1.4	1.4
$\overline{\Delta T}$	**	1.4	1.3	1.4	1.4	1.3	1.3
6 $\overline{\Delta B}$	**	2.0	2.4	1.4	1.5	1.4	1.4
$\overline{\Delta T}$	**	1.9	2.2	1.3	1.5	1.3	1.2
7 $\overline{\Delta B}$	21.0	1.9	4.1	1.6	1.4	1.3	1.3
$\overline{\Delta T}$	20.5	1.9	4.0	1.5	1.3	1.2	1.2

** Error too big due to unstable matrix solution

where $\bar{B}_v(p)$ is the fitted Planck intensity profile. The third set of radiances, $R_3(\bar{p}_1)$, was obtained from Eq. (3.2) using the coefficients obtained in the forward analysis. The "surface contribution" in this case is obtained from the difference between $R_3(\bar{p}_1)$ and the atmospheric contribution to the radiance as follows:

$R_3(\bar{p}_1)$ (Surface Contribution)

$$= R_3(\bar{p}_1) - \int_0^{p_s} \bar{B}_v(p) W_v(\kappa_1, p/\bar{p}_1) dp/p \quad (3.15)$$

A comparison of $R_1(\bar{p}_1)$ and $R_2(\bar{p}_1)$ will reveal the effect of errors in $B_v(p)$ for $p < p_s$, while the difference between $R_2(\bar{p}_1)$ and $R_3(\bar{p}_1)$ will show the impact of the irregular behavior of $\bar{B}_v(p)$ for $p > p_s$. Table 6 lists the radiances that have been computed for the first seven HIRS channels, where the numbers in parentheses are associated with surface contributions. The errors in radiances produced by $\bar{B}_v(p)$ for $p < p_s$ are generally less than 5 erg/cm²/sec/cm⁻¹/sr. The larger differences for the first three channels are due to the fitting errors in $\bar{B}_v(p)$ in the stratosphere. Surface contributions are significant for the last three channels leading to different $R_2(\bar{p}_1)$ and $R_3(\bar{p}_1)$. This is because $\bar{B}_v(p)$ behaves irregularly for $p > p_s$, where the values of weighting functions are still comparable to the peak value. Clearly, errors will be generated in the temperature retrieval due to the limitation of the functional form associated with $\bar{B}_v(p)$. Thus the second problem can be stated as follows: "Due to the irregular behavior of the fitted functional form of $\bar{B}_v(p)$, retrieved temperatures near the surface and in the stratosphere will suffer large errors."

To make the OMM a feasible scheme for temperature retrievals, certain modifications or adjustments are required in order to circumvent the preceding problems.

Table 6. The radiances for the first seven HIRS channels, where the numbers in parentheses are the respective surface contributions. The unit of radiances is $\text{erg/cm}^2/\text{sec/cm}^{-1}/\text{sr}$.

Channel	1	2	3	4	5	6	7
κ	0.49	1.56	1.50	2.19	2.34	4.34	3.16
R_1	53.5 (0.0)	46.0 (0.0)	44.4 (0.0)	54.9 (0.0)	60.1 (0.2)	70.6 (9.6)	78.2 (28.4)
R_2	47.6 (0.0)	42.7 (0.0)	37.6 (0.0)	53.8 (0.0)	60.0 (0.2)	70.3 (9.4)	77.4 (27.5)
R_3	48.2 (0.0)	42.7 (0.0)	37.6 (0.0)	54.3 (0.0)	64.7 (4.9)	75.1 (14.2)	67.0 (17.1)

3.5 Application of OMM with Adjustments

Based on the forward analysis described in the previous subsection, we conclude that the problems of the variation in the sharpness index of the fitted weighting function for each channel and the limitation of the functional form used are the two major sources of errors. The latter problem is also due to the limitation of the OMM, which is developed under the assumption of an infinite atmosphere. To ameliorate the preceding problems, measured radiances must be adjusted. We define a set of adjusted radiances as follows:

$$R_{ij} = \phi_{ij} R_i, \quad (3.16)$$

where R_i is the measured i th channel radiance, and ϕ_{ij} the scaling factor for the i th channel and the j th sharpness index. The scaling factors are introduced to modify the measured radiances by taking into account both the effect of the surface contribution and the variation in the sharpness index. The proper

introduction of scaling factors are critical to the success of the retrieval and can be approximately calculated by:

$$\phi_{ij} = R_{ij}^*/R_i^* \quad , \quad (3.17)$$

where R_{ij}^* denotes the synthetic radiance computed from Eq. (3.2), in which the coefficients are those determined in the forward analysis for the i th channel and the j th sharpness index, and R_i^* is the synthetic radiance computed from Eq. (3.13), using the Planck intensity profile for the i th channel and weighting function. In this way, the irregular behavior of the PH function for $p > p_s$ and the variation in the sharpness index can be removed in the retrieval analysis. Note that ϕ_{ij} also depends on the spectral properties and atmospheric temperature profile. Table 7 lists the values of ϕ_{ij} based on the spectral properties of the HIRS channels and the US Standard Temperature Profile. The fitting of the Planck intensity for $\kappa = 0.49$ ($j=1$) is poor. Thus only the last six sharpness indices were used in the analysis. We notice that $\phi_{ij} < 1.00$ for $i = 1-3$. This is because the PH function is unable to simulate the stratospheric Planck intensity profile for $p < \bar{p}_i$. For $i = 4$ and 5, ϕ_{ij} values are close to 1 in view of the fact that the stratospheric and surface contributions to the radiances are small. For $i = 6$ and 7, surface effects are significant and become dominating for $j = 2$ and 3. Some of the adjusted radiances may not be realistic. Nevertheless, they can be used in a consistent manner in the context of the OMM to obtain reasonable Planck profiles at the desired pressure levels.

For the j th sharpness index, the adjusted radiances R_{ij} are fitted to the PH function, using the prescribed values of m_1 and m_2 . The coefficients r_1 , r_2 , L_1 , and L_2 are subsequently computed. These coefficients are used to compute the Planck intensity profiles according to Eq. (3.9). From each Planck intensity

Table 7. Values of the scaling factor, ϕ_{ij} , based on the channel properties of seven HIRS channels and US Standard Temperature Profile. The channel and sharpness index are denoted by i and j , respectively.

i/j	2	3	4	5	6	7
1	0.787	0.788	0.818	0.810	0.821	0.824
2	0.928	0.929	0.947	0.922	0.920	0.915
3	0.989	0.847	0.938	0.918	0.929	0.936
4	1.060	1.080	0.989	1.000	0.925	0.959
5	1.050	0.999	1.080	1.080	1.010	1.050
6	0.589	0.192	0.931	0.971	1.070	1.040
7	0	0	0.585	0.639	0.964	0.857

profile, a temperature profile can be obtained. The weighted mean temperature profile is then computed from Eq. (3.10). Figure 4 shows the retrieved temperature profile using the values of ϕ_{ij} listed in Table 7 and the synthetic radiances, R_1 , listed in Table 6. Comparing Figs. 4 and 3, we notice that the profile derived from the adjusted radiances is much more improved in accuracy than that derived from the original synthetic radiances. The rms error for $p > 34.7$ mb is 1.92 K, and for $p > 250$ mb, it is about 1.71 K. The maximum error occurs near the tropopause (~ 4.5 K) due to the failure of PH function to fit exactly the simulated radiance minima. The preceding temperature retrieval results using the OMM appear to be encouraging.

In order to test the method on a variety of atmospheric conditions, we also performed retrievals using synthetic radiances using tropical and sub-arctic winter climatological temperature profiles (McClatchey, 1971). In each case, two sets of scaling factors are used. One is the set listed in Table 7 (standard scaling factor), while the other is the set from synthetic studies based on

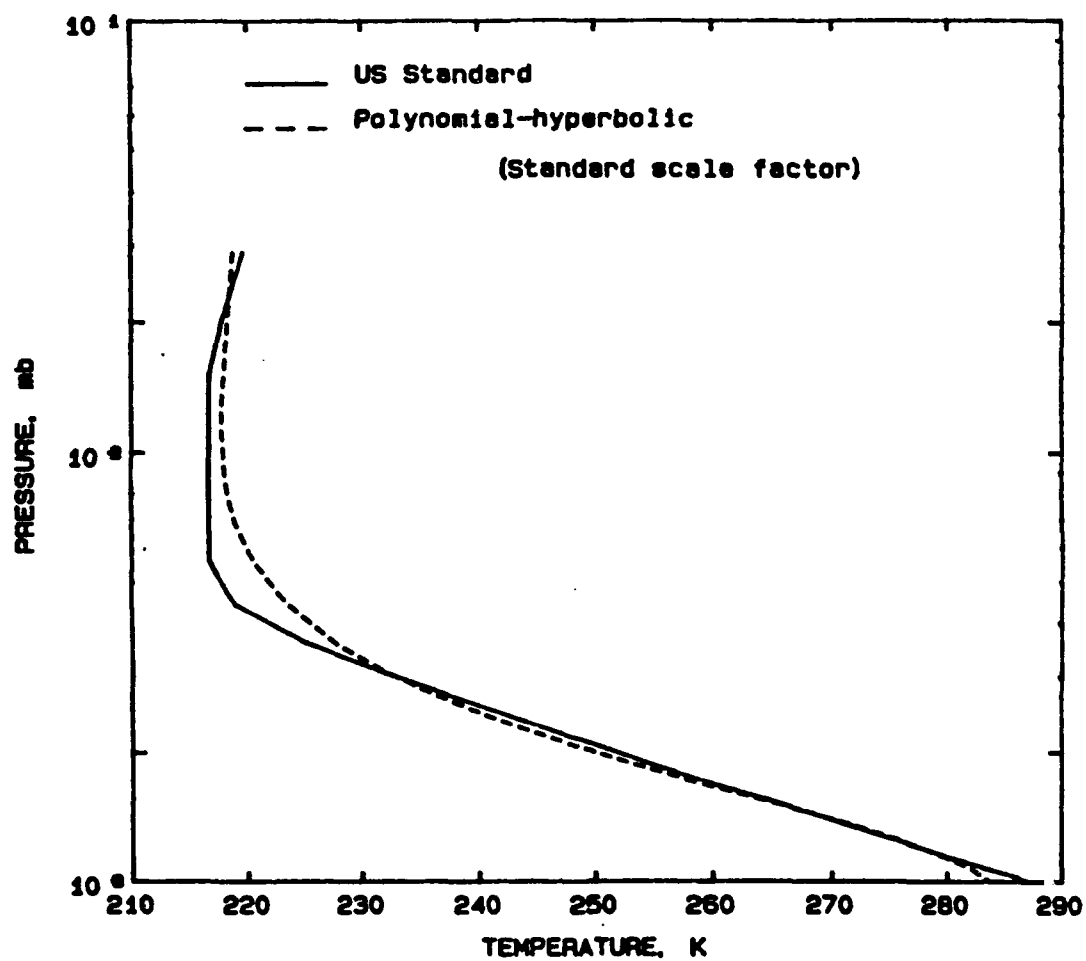


Fig. 4. Retrieved temperature profiles using the adjusted synthetic radiances. The scaling factor set is derived using the US Standard Atmosphere.

respective climatological profiles. Figures 5a and b show retrieval results for tropical and sub-arctic winter atmospheres, respectively. The input climatological profiles are also shown for comparison purposes. As expected, results using the climatological scaling factors are more accurate than those using standard scaling factors. The rms error for tropical atmosphere is 2.36 K using tropical scaling factors for $p > 250$ mb. It is 4.77 K using standard scaling factors. For sub-arctic winter atmosphere we find the rms errors of 1.87 K and 2.58 K, using climatological and standard scaling factors, respectively. In the case of the tropical atmosphere, serious errors occur near the tropopause where there is a strong temperature inversion. As mentioned earlier, the PH function in the present form cannot properly simulate the minima in radiances. However, the retrieved temperature profile in the lower troposphere using the scaling factors is quite reasonable.

Future efforts should be focused on the investigation of the physical basis of scaling factors, and the development of correlations between radiances and scaling factors before this novel method can be applied to real data.

3.6 Optimum Functional Form for the Planck Profile

Based on the previous forward analysis, it is desirable to find a functional form that can better simulate the Planck profile, particularly under the surface ($p > p_s$). Since the temperature is assumed to be constant for $p > p_s$, the Planck intensity for $p > p_s$ is also constant. If we subtract the surface Planck intensity value from the Planck profile, we obtain a reduced Planck profile that will be zero for $p > p_s$. In mathematical terms, we write

$$B'_p(p) = B_p(p) - B_p(p_s) \quad (3.18)$$

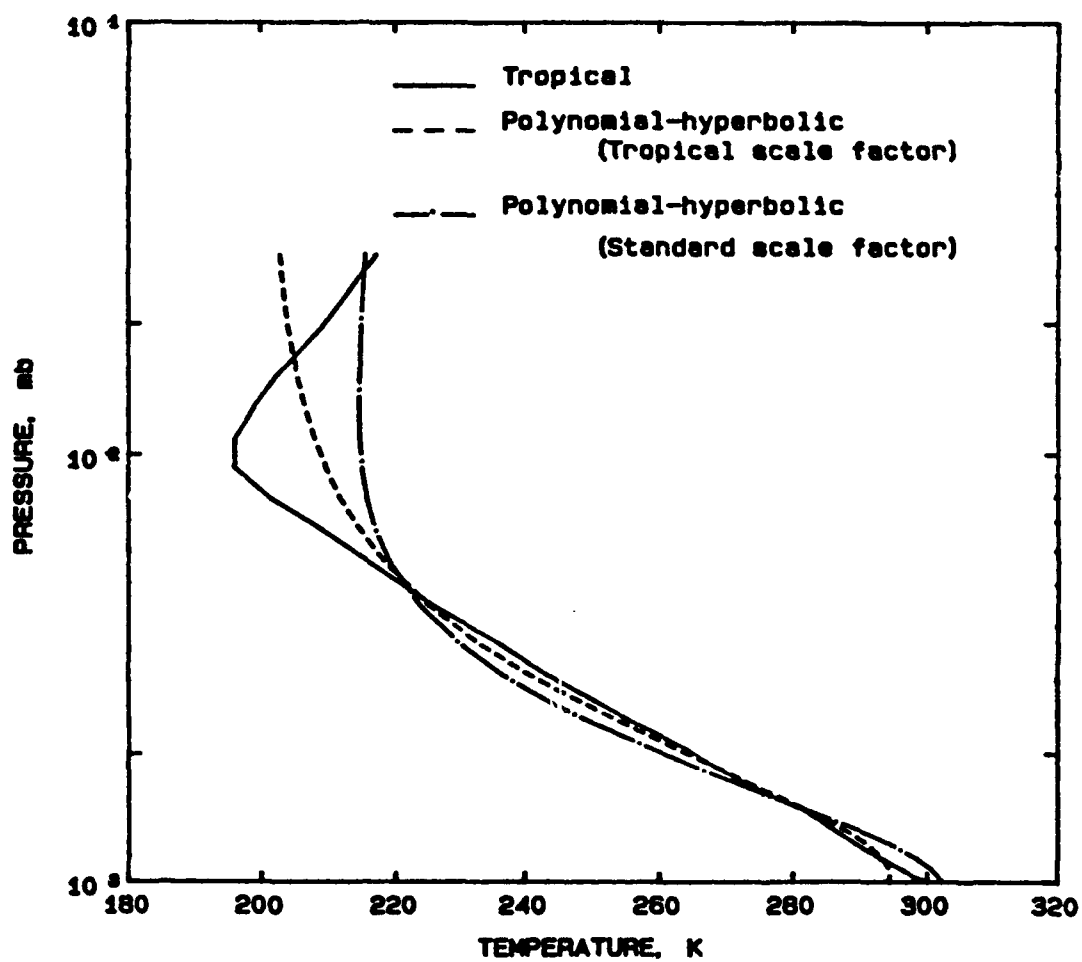


Fig. 5(a). Same as Fig. 4, except for the tropical atmosphere. The scaling factor sets are derived based on the US Standard Atmosphere (dashed-dot curve) and climatological profiles (dashed curve).

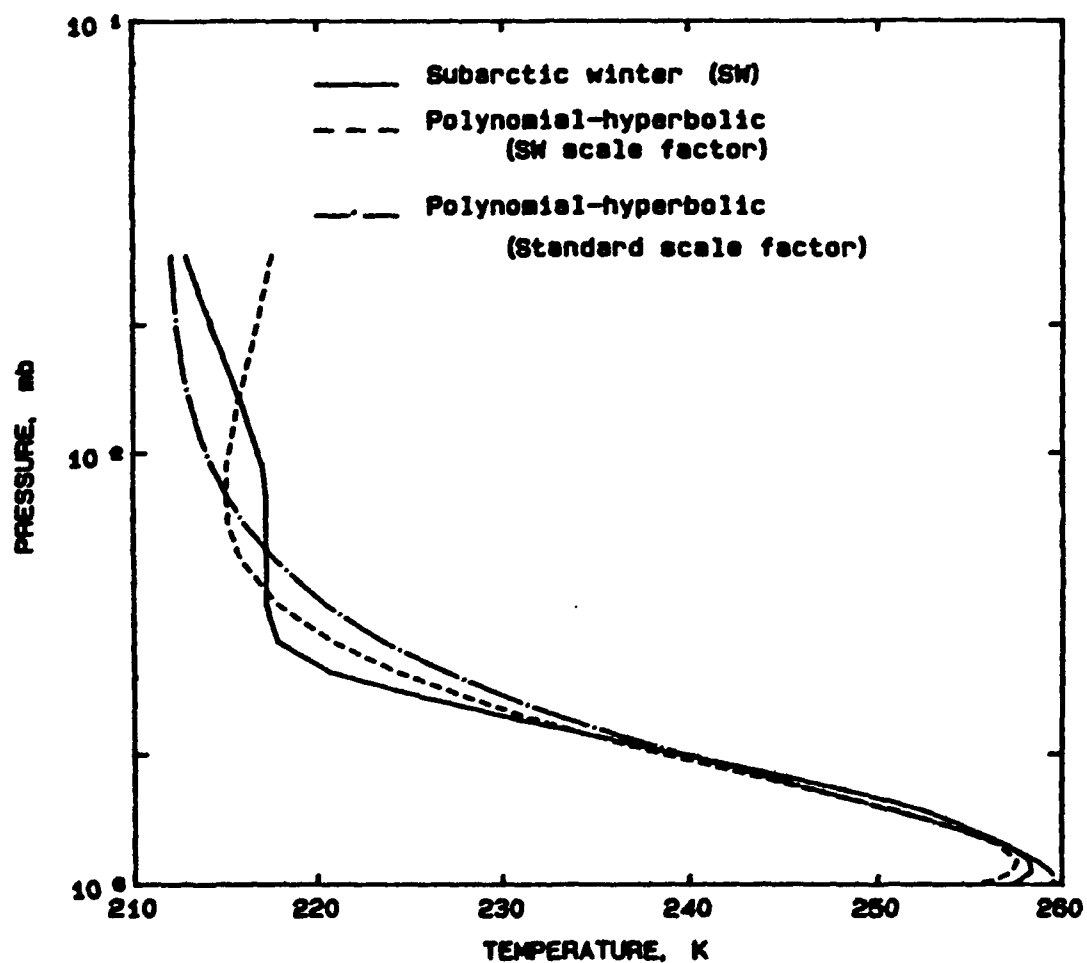


Fig. 5(b). Same as Fig. 5(a), except for the sub-arctic atmosphere.

It follows that $B_{\nu}^L(p) = 0$, for $p > p_s$. This indicates that, in order to fit $B_{\nu}^L(p)$, we must find a functional form that approaches zero for $p > p_s$. Many mathematical functions are qualified for this purpose. However, for the purpose of minimizing error propagation, we shall use the weighting function as our functional form (Rodgers, 1976). The reduced Planck intensity may be expressed in terms of the weighting function in the form

$$B_{\nu}'(p) = \sum_{j=1}^N b_j W_{\nu}(\kappa_j, \bar{p}_j, p) \quad (3.19)$$

The advantage of using the weighting function as the base function for the Planck profile is that the propagation of errors in the radiances into the retrieved Planck profile is minimized. This is demonstrated below. If we express B_{ν} as a linear combination of arbitrary functional forms such that

$$B_{\nu}(p) = \sum_{j=1}^N b_j K(\bar{p}_j, p) \quad (3.20)$$

for discrete values \bar{p}_1 , from Eq. (2.3) we have

$$R(\bar{p}_1) = \sum_{j=1}^N A_{1j} b_j \quad (3.21)$$

where

$$A_{1j} = \int_0^{\infty} K(\bar{p}_j, p) W_{\nu}(\bar{p}_1, p) dp \quad (3.22)$$

However, since b_j is related to B_{ν} via Eq. (3.20), we may express B_{ν} in terms of R . Combining Eqs. (3.20) and (3.21), we obtain

$$B_{\nu}(p) = \sum_{i=1}^N \sum_{j=1}^N [A_{ij}]^{-1} K(\bar{p}_j, p) R(\bar{p}_i) \quad (3.23)$$

where $[A_{ij}]^{-1}$ is the element of the inverse of matrix, $[A_{ij}]$. By denoting

$$D_i(p) = \sum_{j=1}^N [A_{ij}]^{-1} K(\bar{p}_j, p) \quad (3.24)$$

we have

$$B_{\bar{p}}(p) = \sum_{i=1}^N D_i(p) R(\bar{p}) \quad (3.25)$$

Thus, if we minimize $D_i(p)$, the propagation of noise in $R(p)$ into $B_{\bar{p}}(p)$ would be reduced to a minimum. There is one constraint, however. For the retrieved Planck profile to be exact at discrete points, we must have

$$\int_0^{\infty} D_i(p) W_{\bar{p}}(\bar{p}_j, p) dp = \delta_{ij} \quad (3.26)$$

where δ_{ij} is the Kronecker delta function. By jointly minimizing every element of $D_i^2(p)$, subject to the constraint expressed by Eq. (3.26), the best value of $D_i(p)$ may be found using the calculus of variation in the form

$$D_i(p) = \sum_{j=1}^N [W_{ij}^*]^{-1} W(\bar{p}_j, p) \quad (3.27)$$

where

$$W_{ij}^* = \int_0^{\infty} W_{\bar{p}}(\bar{p}_j, p) W_{\bar{p}}(\bar{p}_i, p) dp \quad (3.28)$$

and $[W_{ij}^*]^{-1}$ is the element of the inverse of matrix, W_{ij}^* .

By comparing Eqs. (3.24) and (3.27) along with Eqs. (3.22) and (3.28), it is clear that if

$$K(\bar{p}_j, p) = W_{\bar{p}}(\bar{p}_j, p) \quad (3.29)$$

the propagation of errors in the radiances into the retrieved profile will be

minimized, since Eq. (3.29) satisfies the requirement of minimization as shown in Eq. (3.27).

Section 4

COMPARISONS BETWEEN DIM AND OMM

In this section, we shall first demonstrate that the DIM and OMM for temperature retrievals are equivalent. Preliminary results on the application of the DIM to real-time radiance data set obtained from polar-orbiting satellites are then presented.

4.1 On the Equivalence Between DIM and OMM

The basic theory of the OMM has been described in Section 2. The radiances can be expressed in terms of a polynomial function of \bar{p} as shown in Eq. (2.1). The Planck function can then be computed from Eq. (2.7) using this function. We shall begin with Eq. (2.1) and derive Eq. (2.7) using the DIM. Since the DIM is basically a method of linear transformation, we single out an arbitrary term of the n th power of \bar{p} in the radiance expression for the sake of clarity. We will attempt to show that the Planck function can be expressed in terms of the n th power of \bar{p} . We may write

$$R(\bar{p}) = \bar{p}^n \quad (4.1)$$

Using the OMM, the corresponding Planck function is

$$B(p) = \left[\int_0^\infty \bar{p}^{n-1} W_p(\bar{p}) d\bar{p} \right]^{-1} p^n \quad (4.2)$$

Define

$$\bar{p} = e^{-y} \quad \text{or} \quad y = -\ln \bar{p} \quad (4.3)$$

so that Eq. (4.1) can be rewritten as

$$R(y) = e^{-ny} \quad (4.4)$$

According to the theory of the DIM, the Planck function can be expressed as the linear sum of higher-order derivatives of R with respect to the logarithm of pressure as follows:

$$B(x) = \sum_{j=0}^{\infty} \lambda_j \frac{d^j R(x)}{dx^j} \quad (4.5)$$

where

$$x = -\ln p \quad (4.6)$$

and λ_j are coefficients obtained by the Laplace transform. Since R is an exponential function, its higher-order derivatives are given by:

$$\frac{d^j R(x)}{dx^j} = (-n)^j e^{-nx} \quad (4.7)$$

On substituting Eq. (4.7) into Eq. (4.5), we obtain

$$B(x) = c e^{-nx} \quad (4.8)$$

where

$$c = \sum_{j=0}^{\infty} \lambda_j (-n)^j \quad (4.9)$$

In order to have an analytic expression for λ_j , Eq. (4.2) may be written as a bilateral Laplace transform as follows:

$$w(-s) = \int_{-\infty}^{\infty} e^{sy} W(y) dy \quad (4.10)$$

where s is a transform parameter. We then expand $1/w(-s)$ into a McLaurin series in the form

$$[w(-s)]^{-1} = \sum_{k=0}^{\infty} \lambda_k s^k, \quad (4.11)$$

with

$$\lambda_k = [w(-s)]_{s=0}^{[k]} / k! \quad (4.12)$$

Comparing Eq. (4.11) with Eq. (4.9), we find

$$c = [w(-n)]^{-1} \quad (4.13)$$

Using Eq. (4.10), we obtain

$$c = \left[\int_0^{\infty} \tilde{p}^{n-1} w_{\tilde{p}}(\tilde{p}) d\tilde{p} \right]^{-1} \quad (4.14)$$

Since $e^{-nx} = p^n$, Eq. (4.8) is identical to Eq. (4.2). We have showed that the DIM is equivalent to the OMM. Further, we may also compute the coefficients λ_j from known values of c by a matrix inversion.

In an attempt to provide mathematically more rigorous proof of the uniqueness of the solution of either the DIM or the OMM, Liao (1989) showed that the convolution transforms arising from geophysics, such as Eq. (2.3), are of the Laguerre-Pólya class. The special characteristics of the Laguerre-Pólya class is that its inversion function is the convergence limit of any sequence of polynomials having real roots only. It follows that a unique solution can be obtained for the convolution transform whose kernel can be shown to belong to such a class. Details are given in the form of a short research note in the Appendix.

In our previous work (Liou and Ou, 1989), we used a polynomial in $\ln p$ (instead of p) to fit radiances. The retrieved temperature profile based on a polynomial in $\ln p$ (Fig. 7 in Liou and Ou, 1989) is more satisfactory than that based on a polynomial in p (Fig. 3) for $p > 250$ mb. However, for $p < 250$ mb, the

DIM also suffered large errors. Apparently the DIM depends less on the surface contribution. To understand the reason as to why the DIM works better in the temperature retrieval, we perform analysis on the behavior of the fitted Planck function for $p > p_s$.

By fitting the radiances using the n th power in $-\ln \bar{p}$, we have

$$R(-\ln \bar{p}) = (-\ln \bar{p})^n \quad (4.15)$$

The Planck function is then given by

$$B(-\ln p) = \sum_{j=0}^n \zeta_j (-\ln p)^j \quad (4.16)$$

where ζ_j 's are coefficients to be determined. The Planck function is also a polynomial in $\ln p$. The Planck function profile of HIRS Channel 7 is fitted to 4th-degree polynomials both in p and $\ln p$, as shown in Fig. 6. The fitting in both cases are quite satisfactory above the surface. However, below the surface the fitting in $\ln p$ is much closer to an isothermal profile than that in p . Also shown in the figure is the generalized weighting function of Channel 7, which has significant contribution for $p > 1000$ mb. For this reason, the behavior of the fitting for $p > p_s$ will greatly affect the radiance of Channel 7. The preceding analysis explains why the DIM performs better than the OMM near the surface.

4.2 Preliminary Applications of the DIM to HIRS Data

We have shown that the OMM needs modifications in order to be practical in temperature retrievals and that the DIM is better than the OMM. We have made an attempt to investigate the applicability of the DIM to the inference of atmospheric temperatures using real-time data.

An archive of 3473 collocated clear-sky temperature profiles and radiance

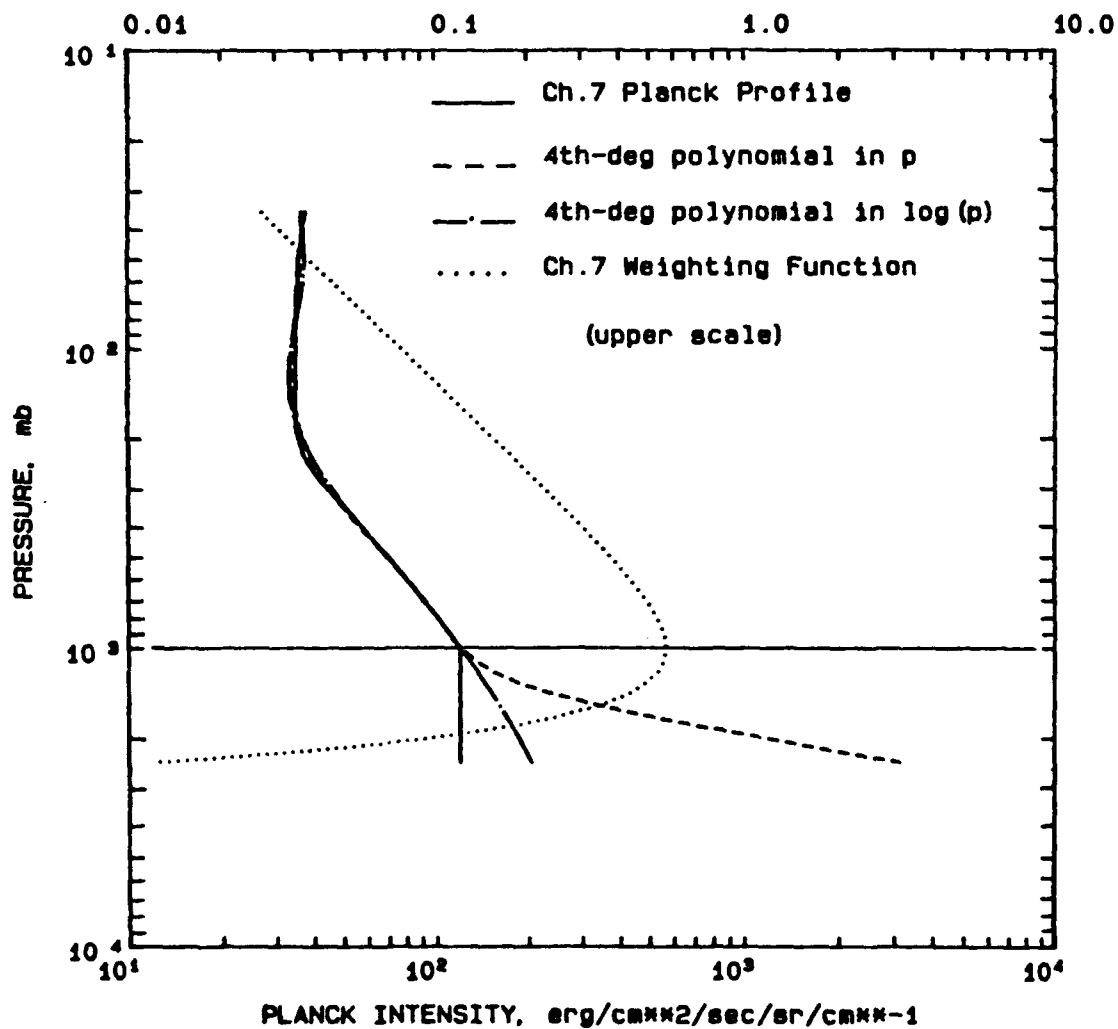


Fig. 6. The fitting of 4th-order polynomials in pressure (dashed curve) and in logarithm of pressure (dashed-dot curve) to the Channel 7 Planck intensity profile (solid curve) using the US Standard Atmosphere. Also shown is the Channel 7 weighting function.

data sets (kindly provided to us by Dr. L. McMillin) were used to perform the retrieval analysis. The temperature profiles were based on local sounding, while the radiance data were obtained from HIRS instruments on board NOAA 10 polar-orbiting satellites. For each profile, the latitude, longitude, time, date, land or sea, solar zenith angle, and water vapor mixing ratio profile are also specified. The data are randomly distributed over lands and oceans. There were 1964 cases over lands and 1509 cases over oceans. The data were largely obtained between March 21 and April 10, 1987. All the cases correspond predominantly to clear atmospheres with a minimum amount of cloud contamination. Temperature soundings over land were obtained from land stations. Sounding over the oceans were obtained from coastal stations, island stations, platforms, and ships. The observed radiances are corrected to the nadir direction.

To perform retrieval exercises, we first convert the brightness temperature values of Channels 1-7 to radiances, we then follow the procedures outlined by Liou and Ou (1989) to obtain the retrieved temperature profile. The retrieved results are compared with co-located sounding profiles. Specifically, temperature values at the peak pressure level of the weighting functions are selected and analyzed. In general, the rms errors at each pressure level is about the same magnitude as the error from the previous synthetic computations (Liou and Ou, 1988). The rms errors at the lower four pressure levels are on the order of 2-5 K. The rms errors at the lowest pressure level (1000 mb) are about 3 K. The cause for this error is produced by the problem of the surface discontinuity.

Figure 7 shows the retrieved temperature vs. sounding temperatures at 1000 mb. There are about 728 points, which were all located between 30°N and 60°N. The straight line denotes that the two temperatures are equal. Most of the data

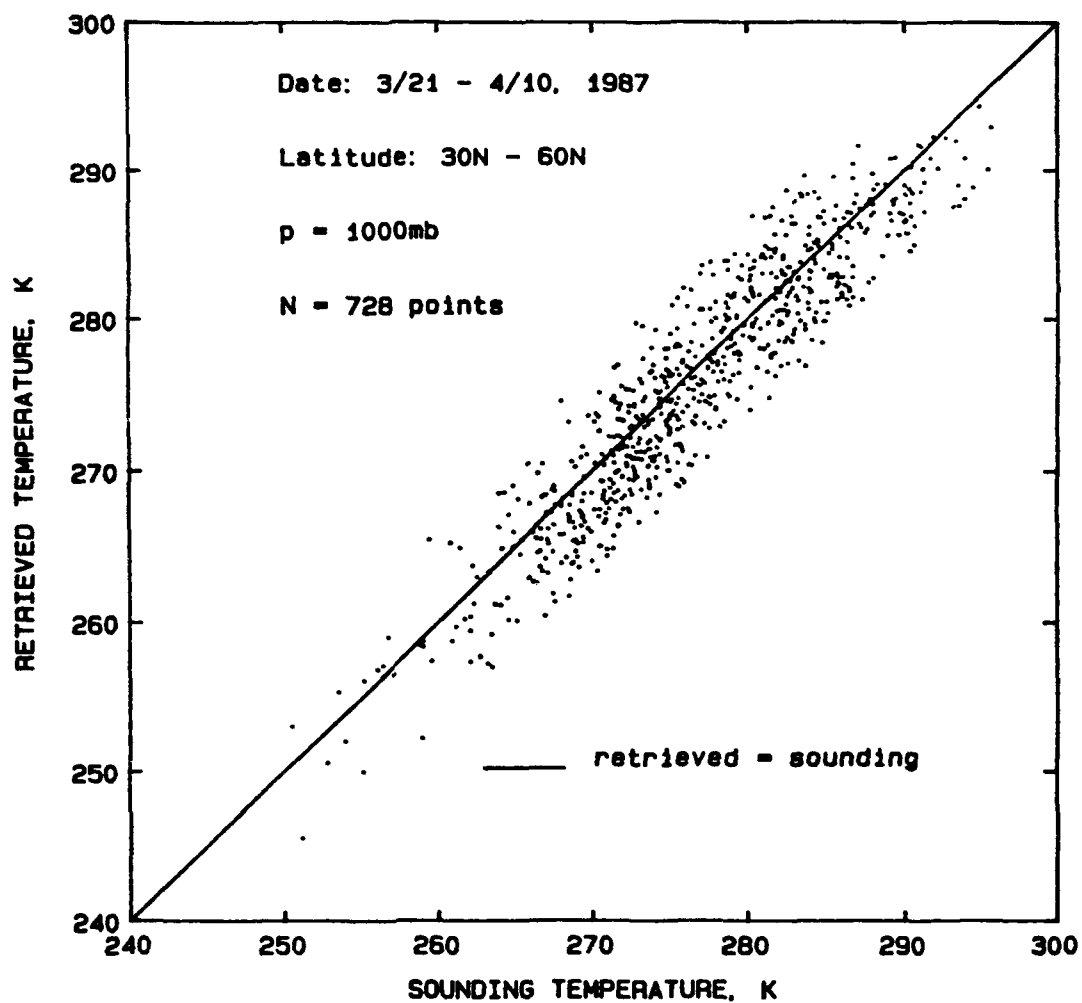


Fig. 7. The retrieved temperatures vs. the sounding temperatures at 1000 mb. The radiance data were collected from NOAA 9 during the period between March 21 to April 10, 1987, and distributed in the latitude zone between 30°N and 60°N. The straight line represents that the retrieved temperature is equal to the sounding temperature.

points fall close to the line. The correlation coefficient is 0.93. The errors of its individual points can be attributed to the combined effects of many factors. These include the topographic effects, cloud contamination, uncertainty of the water vapor contamination in the radiances of Channel 6 and 7, errors in the weighting function due to different temperature profiles, errors generated due to a least-square fitting of weighting functions, errors in the fitting of radiances, etc.

In order to improve the performance of the DIM, it is necessary to undertake modifications and refinements of the methodology similar to those described in Section 3.

Section 5

CONCLUSIONS

In this report, we first present the basic theory involving the OMM. It is shown that the Planck function profile can be directly related to the upwelling radiance through polynomial expansions in the pressure coordinates. In order to perform temperature retrievals, an optical number system has been constructed based on the generalized weighting function. A specific form for the OMM has been developed based on the fitting of non-linear hyperbolic functions to the measured radiances. The inferred Planck profile is shown to be the combination of the optical exponential function.

We apply the OMM to the retrieval of temperature profiles using the HIRS-2 channel in the $15\text{ }\mu\text{m}$ CO_2 band. The radiances are calculated based on the spectral properties of seven channels using the US Standard Atmosphere profile. They are subsequently fitted to both a 5th-degree polynomial and a combined polynomial-hyperbolic (PH) function. Retrieved temperature profiles in both cases deviate significantly from the standard temperature profile. The profile derived from the PH function is better than that from the polynomial. A further examination reveals that the retrieved temperatures using the PH function are colder by 5-12 K and warmer by 0-5 K below and above 250 mb, respectively.

To investigate the reasons for large deviations in the retrieved temperature profile, we perform a forward analysis. A combination of a linear function and two terms of the optical exponential function are fitted to the Planck profile. For smaller sharpness indices, i.e., broader weighting function, the fitting is poor and produces large rms errors in the retrieved temperature profiles. For sharpness indices larger than 2.0, the rms errors are on the order of 1.2-2.0 K.

In the forward analysis, we also identify two problems, which are the major reasons for the deviation of the retrieved temperature profile. The first problem is associated with the variation of the sharpness index with the sensor channels. Fitting all the radiances to the PH function using only one set of coefficients is mathematically inconsistent. This problem can be seen from the variation pattern in the coefficients of the PH function for different sharpness indices. The second problem is caused by the irregular behavior of the fitted Planck profile for $p > p_s$, using the optical exponential function. The retrieved temperatures suffer large errors because the below-surface contribution could not be properly accounted for. The below-surface contribution is particularly significant for channels with the weighting function peaks in the lower atmosphere. In view of the above, certain modifications on the OMM or adjustments to the measured radiances are necessary in order for this method to be a practical scheme for temperature retrievals.

We have developed a scheme to adjust and augment the measured radiances through a set of scaling factors, which includes the effects of the sharpness index variation, surface discontinuity, channel characteristics, and functional forms. We show that mathematically consistent retrievals can be performed on the adjusted radiances to obtain an optimum functional form, which is most effective in simulating the Planck profile and minimizing the error propagation.

Through a simple derivation following the fundamental principles of the DIM, we show that the DIM and OMM are mathematically equivalent. A rigorous proof on the uniqueness of the solution of both methods is also given. However, in our previous work (Liou and Ou, 1988), we demonstrated that retrieved temperatures based on synthetic computations using the DIM are within about 3 K. However, in the present work, the retrieved temperature results using the OMM without

adjustments are less satisfactory. The superiority of the DIM is due to the fact that it was the radiance polynomial fitting in $\ln p$, whereas the OMM uses that in p . The fitting in the $\ln p$ coordinate accounts for some surface contributions to the radiances. Finally, we apply the DIM to an archive of 3473 collocated temperature profiles and HIRS radiance data sets from NOAA 9. The accuracy of the retrieved temperature profiles is within about 3 K, which is comparable to that obtained from synthetic analyses.

REFERENCES

- Chandrasekhar, S., 1950: Radiative Transfer. Clarendon Press/Oxford, 393 pp.
- Chou, M.D. and L. Kouvaris, 1986: Monochromatic calculations of atmospheric radiative transfer due to molecular line absorption. *J. Geophys. Res.*, 91, 4047-4055.
- King, J.I.F., 1985: Theory and application of differential inversion to remote temperature sensing. In Advances in Remote Sensing Retrieval Methods, A. Deepak, H.E. Fleming and M.T. Chahine (Eds.), Deepak Publishing Co., N.Y., 437-444.
- King, J.I.F., 1987: Private communication.
- Leon, S. and J.I.F. King, 1989: A smart algorithm for nonlinear interpolation and noise discrimination. In RSRM '87, Advances in Remote Sensing Retrieval Methods, A. Deepak, H.E. Fleming and J.S. Theon (Eds.), Deepak Publishing Co., N.Y., 157-163.
- Liao, G., 1990: A class of Laguerre-Pólya kernel and application to atmospheric temperature retrieval. SIAM (submitted).
- Liou, K.N. and S.C. Ou, 1988: Remote sounding of atmospheric temperature profiles using the differential inversion method. Report AFLG-TR-88-0152. Air Force Geophysical Laboratory, Hanscom AFB, MA 01731, 48 pp. ADA199896.
- Liou, K.N., S.C. Ou, and J.I.F. King, 1989: On the differential inversion method of temperature retrievals. In RSRM '87, Advances in Remote Sensing Retrieval Methods, A. Deepak, H.E. Fleming and J.S. Theon (Eds.), Deepak Publishing Co., N.Y., 143-156.
- Phillips, N., J. Susskind, and L. McMillin, 1988: Results of a Joint NOAA/NASA Sounder Simulation Study. *J. Atmos. Ocean Tech.*, 5, 44-56.
- Rothman, L.S., R.R. Gamache, A. Barbe, A. Goldman, J.R. Gillis, L.R. Brown, R.A. Toth, J.M. Flaud and C. Camy-Peyret, 1983: AFGL atmospheric line parameters compilation: 1982 edition. *Appl. Opt.*, 22, 2247-2256.
- Smith, W.L., 1970: Iterative solution of the radiative transfer equation for the temperature and absorbing gas profile of an atmosphere. *Appl. Opt.*, 9, 1993-1999.

APPENDIX

A Class of Laguerre-Pólya Kernel and Application to Atmospheric Temperature Retrieval

G. Liao*

Department of Mathematics
University of Utah
Salt Lake City, Utah 84112

*Current Address: Department of Mathematics
University of Texas at Arlington
Arlington, Texas 76019

ABSTRACT

A class of convolution transforms (generalized Laplace transforms) arising from geophysics are shown to be Laguerre-Pólya, i.e., their inversion function is the limit of real polynomials whose roots are all real. It follows that, by applying Widder's theory, the convolution transforms can be inverted by using operational calculus.

ACKNOWLEDGEMENTS

This work was supported by the Geophysics Laboratory under contract F-19628-88-K-0049. The author thanks Professor K. N. Liou and Dr. S. C. Ou for many valuable discussions during the preparation of this paper. He is also grateful to Professor Roger Bernard for making Sheil-Small's work known to him.

Section A.1 Generalized Laplace Transforms

The transforms that we will study are of the form

$$f(x) = \int_{-\infty}^{\infty} N(x-y) g(y) dy, \quad (A.1)$$

where the kernel

$$N(x) = e^x \cdot e^{-m \cdot x/m}, \quad m > 0.$$

To link Eq. (A.1) to the atmospheric temperature retrieval, we refer to King (1985). The mathematical problem is to invert Eq. (A.1), i.e., to determine $g(x)$, given $f(x)$.

The following analysis shows that if $m = 1$, Eq. (A.1) reduces to the unilateral Laplace transform, which is usually given by

$$\psi(s) = \int_0^{\infty} e^{-st} \gamma(t) dt. \quad (A.2)$$

To see this, let $s = e^x$, and $t = e^{-y}$. Then $dt = -e^{-y} dy$, and

$$\psi(e^x) = \int_{-\infty}^{\infty} e^{-e^x \cdot e^{-y}} \cdot \gamma(e^{-y}) \cdot e^{-y} dy. \quad (A.3)$$

Thus

$$e^x \psi(e^x) = \int_{-\infty}^{\infty} e^{x-y} \cdot e^{-e^{x-y}} \cdot \gamma(e^{-y}) dy.$$

Section A.2 Laguerre-Pólya Class

Definition: The reciprocal of the bilateral Laplace transform of the convolution kernel, N , is called the inversion function of the convolution transform.

To compute the inversion function, $E(s)$, of Eq. (A.1), we take the Laplace transform as follows:

$$\begin{aligned} \frac{1}{E(s)} &= \int_{-\infty}^{\infty} e^{-sx} e^x e^{-me^{x/m}} dx \\ &= \int_0^{\infty} m^{ms-m+1} v^{m-ms-1} e^{-v} dv \end{aligned} \quad (A.4)$$

by variable transformation $v = m e^{x/m}$. Hence

$$E(s) = \frac{m^{-ms-m+1}}{\Gamma[m(1-s)]}.$$

In particular, if $m = 1$, then

$$E(s) = \frac{1}{\Gamma(1-s)} \quad (A.5)$$

Since

$$\frac{1}{\Gamma(s)\Gamma(1-s)} = \frac{\sin \pi s}{\pi s} = s \prod_{k=1}^{\infty} \left(1 - \frac{s^2}{k^2} \right),$$

and

$$\Gamma(s)^{-1} = e^{\gamma s} s \prod_{k=1}^{\infty} \left(1 + \frac{s}{k} \right) e^{-s/k},$$

we have the well-known product expansion

$$E(s) = \frac{1}{\Gamma(1-s)} = e^{-\gamma s} \prod_{k=1}^{\infty} \left(1 - \frac{s}{k}\right) e^{s/k},$$

where γ is Euler's constant:

$$\gamma = \lim_{n \rightarrow \infty} \left(\sum_{k=1}^n \frac{1}{k} - \log n \right).$$

Definition: An entire function, $E(s)$, is said to belong to the Laguerre-Pólya class if it can be expressed as

$$E(s) = a \cdot \exp(bs - cs^2) \cdot s^p \cdot \prod_{k=1}^{\infty} \left(1 - \frac{s}{A_k}\right) \exp\left(\frac{s}{A_k}\right), \quad (A.6)$$

where a , b , c , and A_k are real, $C > 0$, p is a non-negative integer, and

$$\sum_{k=1}^{\infty} \frac{1}{A_k^2} < \infty.$$

Clearly, $E(s) = \frac{1}{\Gamma(1-s)}$ is Laguerre-Pólya.

The inversion problem could be solved if the inversion function, $E(s)$, belongs to the Laguerre-Pólya class as follows (Widder, 1971). Replace s in $E(s)$ by the differentiation, D , to get a differential operator, $E(D)$. The function $g(x)$ can be determined by

$$g(x) = E(D) f(x)$$

in the sense of operational calculus.

Section A.3 The Inversion Function

As computed in Section A.2, the inversion function $E(s)$ for Eq. (A.1) is given by

$$E(s) = \frac{m^{-ms} + m - 1}{\Gamma(m(1-s))}, \quad m > 0 \quad (A.7)$$

We shall now confirm that $E(s)$ belongs to the Laguerre-Pólya class.

Our argument is based on the criterion described in Sheil-Small (1989, Lemma 4), which says that a real entire function $f(z)$ is in the Laguerre-Pólya class if, and only if, $\text{Im}L(z) \leq 0$ for $z \in H^+$, where $L(z) = f'(z)/f(z)$ and H^+ is the upper half plane.

Proposition: $\text{Im} \frac{E'(s)}{E(s)} < 0$ for $s \in H^+$.

Proof:

$$\begin{aligned} m^{1-m} \cdot E'(s) &= \frac{m^{-ms}(-m)\ln m}{\Gamma(m(1-s))} - \frac{m^{-ms}\Gamma'(m(1-s))(-m)}{\Gamma(m(1-s))^2} \\ &= \frac{m^{-ms}(-m)}{\Gamma(m(1-s))} \left[\ln m - \frac{\Gamma'(m(1-s))}{\Gamma(m(1-s))} \right]. \end{aligned} \quad (A.8)$$

Let $s = x + iy$, $y > 0$. We have

$$\frac{\Gamma'(m(1-s))}{\Gamma(m(1-s))} = -\gamma - \frac{1}{m(1-s)} + \sum_{n=1}^{\infty} \frac{m(1-s)}{n(m(1-s) + n)}, \quad (A.9)$$

where γ is the Euler number. The infinite series on the right side of the equation is absolutely and uniformly convergent in any closed region of H^+ . Substituting Eq. (A.9) into Eq. (A.8), we get

$$\begin{aligned}
\frac{E'(s)}{E(s)} &= -m \left[\ln m - \left(-\gamma - \frac{1}{m(1-s)} + \sum_{n=1}^{\infty} \frac{m(1-s)}{n(m(1-s) + n)} \right) \right] \\
&= -m \left[\ln m + \gamma + \frac{1}{m(1-s)} - \sum_{n=1}^{\infty} \frac{m(1-s)}{n(m(1-s) + n)} \right] \quad (A.10)
\end{aligned}$$

Compute

$$\frac{1}{1-s} = \frac{1}{1-x-iy} = \frac{1-x+iy}{(1-x)^2 + y^2} \quad ,$$

and

$$\begin{aligned}
\operatorname{Im} \frac{1-s}{m(1-s) + n} &= \operatorname{Im} \frac{1-x-iy}{m+n-xm-imy} \\
&= \operatorname{Im} \frac{(1-x-iy)(m+n-xm+imy)}{(m+n-xm)^2 + m^2y^2} \\
&= \frac{(1-x)my - y(m+n-xm)}{(m+n-xm)^2 + m^2y^2} \\
&= \frac{my - mxy - my - yn + mxy}{(m+n-xm)^2 + m^2y^2} \\
&= - \frac{yn}{(m+n-xm)^2 + m^2y^2}
\end{aligned}$$

Thus,

$$\begin{aligned}
\operatorname{Im} \frac{E'(s)}{E(s)} &= \operatorname{Im} \left(\frac{-1}{1-s} + \sum_{n=1}^{\infty} \frac{m}{n} \frac{1-s}{m(1-s) + n} \right) \\
&= - \frac{y}{(1-x)^2 + y^2} + \sum_{n=1}^{\infty} \frac{m}{n} \cdot \frac{-yn}{(m+n-xm)^2 + m^2y^2}
\end{aligned}$$

$$= - \frac{y}{(1-x)^2 + y^2} - \sum_{n=1}^{\infty} \frac{ym}{(m+n-xm)^2 + m^2y^2} < 0$$

if $y > 0$.

REFERENCES

- King, J.I.F., 1985: The inverse solution for remote atmospheric sounding, Advances in Remote Sensing Retrieval Methods, A. Deepak, H.E. Fleming and M.T. Chahine (Eds.), Deepak Publishing Co., N.Y., pp. 437-444.
- Sheil-Small, T., 1989, On the zeros of the derivatives of real entire functions and Siman's conjecture, Annals of Mathematics, vol. 129, pp.179-193.
- Widder, D.V., 1971: An Introduction to Transform Theory, Academic Press, N.Y.